



HAL
open science

Multiple branches of travelling waves for the Gross Pitaevskii equation

David Chiron, Claire Scheid

► **To cite this version:**

David Chiron, Claire Scheid. Multiple branches of travelling waves for the Gross Pitaevskii equation. 2017. hal-01525255v1

HAL Id: hal-01525255

<https://hal.science/hal-01525255v1>

Preprint submitted on 19 May 2017 (v1), last revised 15 Feb 2018 (v3)

HAL is a multi-disciplinary open access archive for the deposit and dissemination of scientific research documents, whether they are published or not. The documents may come from teaching and research institutions in France or abroad, or from public or private research centers.

L'archive ouverte pluridisciplinaire **HAL**, est destinée au dépôt et à la diffusion de documents scientifiques de niveau recherche, publiés ou non, émanant des établissements d'enseignement et de recherche français ou étrangers, des laboratoires publics ou privés.

MULTIPLE BRANCHES OF TRAVELLING WAVES FOR THE GROSS-PITAEVSKII EQUATION

DAVID CHIRON¹ AND CLAIRE SCHEID²

Abstract. Explicit solitary waves are known to exist for the Kadomtsev-Petviashvili-I (KP-I) equation in dimension 2. We first address numerically the question of their Morse index. The results confirm that the lump solitary wave has Morse index one and that the other explicit solutions correspond to excited states. We then turn to the 2D Gross-Pitaevskii (GP) equation which in some long wave regime converges to the (KP-I) equation. Numerical simulations already showed that a branch of travelling waves of (GP) converges to a ground state of (KP-I), expected to be the lump. In this work, we perform numerical simulations showing that the other explicit solitary waves solutions to the (KP-I) equation give rise to new branches of travelling waves of (GP) corresponding to excited states.

1991 Mathematics Subject Classification. 35B38, 35C07, 35J61, 35Q40, 35Q55.

May 19, 2017.

1. MOTIVATIONS

1.1. (NLS) with nonzero condition at infinity

The nonlinear Schrödinger equation (NLS) with nonzero condition at infinity appears in a variety of physical problems: condensed matter physics (see [28]), Bose-Einstein condensates and superfluidity (*cf.* [30], [1]), as well as nonlinear Optics (see [22]). Depending on the physical problem, several nonlinearities may be of interest (see the examples and references quoted in [11, 14]). The most popular one is of cubic type and leads to the well-known Gross Pitaevskii (GP) equation for which NLS equation writes:

$$i\frac{\partial\Psi}{\partial t} + \Delta\Psi = \Psi(|\Psi|^2 - 1). \quad (\text{GP})$$

In this work, we shall consider GP equation in space dimension two and with the following condition at infinity: $|\Psi| \rightarrow 1$ as $|x| \rightarrow +\infty$. The GP equation is the Schrödinger flow associated with the Ginzburg-Landau energy

$$E(u) = \int_{\mathbb{R}^2} |\nabla u|^2 + \frac{1}{2} \int_{\mathbb{R}^2} (|u|^2 - 1)^2.$$

Keywords and phrases: Non Linear Schrödinger equation, travelling waves, Kadomtsev-Petviashvili equation, vortex

¹ Université Côte d'Azur, CNRS, LJAD, France, chiron@unice.fr

² Université Côte d'Azur, Inria, CNRS, LJAD, France, Claire.Scheid@unice.fr

For a nowhere vanishing solution, GP can be recast into a hydrodynamical form, via the Madelung transform $\Psi = \sqrt{\rho}e^{i\varphi}$:

$$\begin{cases} \partial_t \rho + 2\nabla \cdot (\rho \nabla \varphi) = 0 \\ \partial_t \varphi + |\nabla \varphi|^2 + \rho - 1 = \frac{\Delta \sqrt{\rho}}{\sqrt{\rho}}. \end{cases} \quad (1)$$

This is an incompressible irrotational Euler type system with an additional term called quantum pressure in the right-hand side of the second, Bernoulli type, equation. Neglecting the quantum pressure and linearizing around the constant state ($\rho = 1, \varphi = 0$) corresponding to the condition at infinity, one obtains the free wave equation:

$$\begin{cases} \partial_t a + \nabla \cdot V = 0 \\ \partial_t V - 2\nabla a = 0 \end{cases}$$

with $(a, V) = (\sqrt{\rho} - 1, \nabla \varphi)$. This allows for the definition of the speed of sound $\mathbf{c}_s = \sqrt{2}$ (see [1, 28] for details). In this work, we furthermore focus on the travelling waves solutions. We consider the ansatz $\Psi(t, (x_1, x_2)) = u(x_1 - ct, x_2)$, with $(t, x_1, x_2) \in \mathbb{R}^3$, that is representing a wave travelling in the direction x_1 with speed c . The profile u of the travelling wave then solves:

$$ic\partial_{x_1}u - \Delta u + u(|u|^2 - 1) = 0. \quad (\text{TW}_c)$$

The condition at infinity is now $u \rightarrow 1$, up to a phase change. Indeed, it was conjectured in [21] that u tends to 1 at some algebraic rate, and this has been proved (if u has finite energy) in [19].

In addition to E , the momentum is also a conserved quantity, reflecting the invariance by space translation of GP, that is also central to illustrate the qualitative behavior of the travelling waves solutions. For u tending suitably to 1 at infinity, its first component reads

$$P(u) = \int_{\mathbb{R}^2} \langle i(u-1), \partial_{x_1} u \rangle,$$

with $\langle \cdot, \cdot \rangle$ the real scalar product on \mathbb{C} (the second component $\int_{\mathbb{R}^2} \langle i(u-1), \partial_{x_2} u \rangle$ is also conserved but will be useless for the travelling waves propagating in the x_1 direction). The study of the behavior of the energy E and the momentum P with speed c is at the heart of the understanding of (among others) the stability properties of the travelling wave solutions. Thus the Energy *vs* Momentum diagram given as a speed parametrized curve is especially instructive. We refer to the pioneering work of C.A. Jones, P.H. Roberts in two space dimensions and tridimensional axisymmetric for GP in [21] and to the more recent works of [11, 14] for more general nonlinearities. In all these studies, the computed solutions are critical points of the action $\mathcal{F}_c = E - cP$ that are characterized as minimizers of some functional under a single constraint (for instance in [21], the energy is minimized at fixed momentum). Therefore a Morse index of one is expected, i.e. the Hessian of \mathcal{F}_c has only one negative eigenvalue. We recall in figure 1 the diagram for the case of 2D travelling waves of GP (issued from [21]), and we shall call this branch the JR branch. Several mathematical results are known about this JR branch: see [8], [5], [25] (in dimension larger than two) and [13].

In this paper, on the contrary to the previous mentioned references, we propose to numerically investigate the possible existence of solutions to (TW_c) , which may be of Morse index > 1 ; that is excited states. We give a positive answer to this question. As a matter of fact, we obtain that there exists at least 4 new branches of travelling wave solutions in the Energy-Momentum diagram as depicted in figure 2 (the blue branch corresponds to the blue one in figure 1 and is the JR branch). It is highly plausible that there exist many other ones. To construct these new branches, we strongly rely on the knowledge of the asymptotics $c \rightarrow 0$ and $c \rightarrow \mathbf{c}_s$.

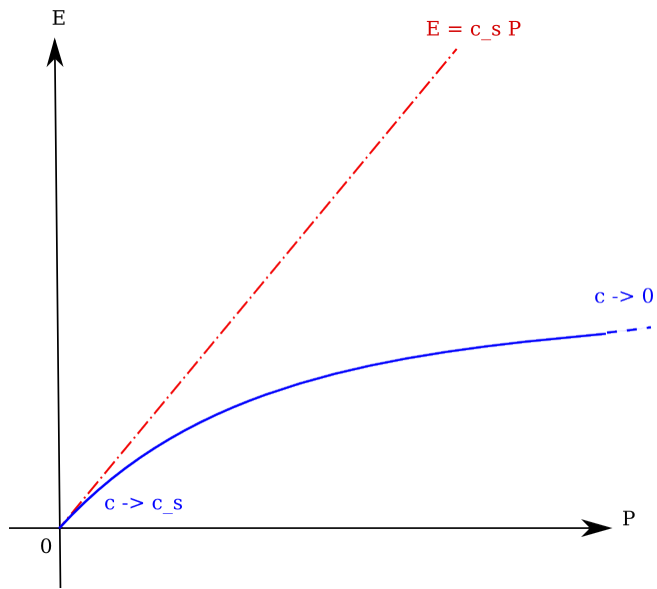


FIGURE 1. Energy-Momentum diagram for 2D travelling waves of GP: the Jones-Roberts branch

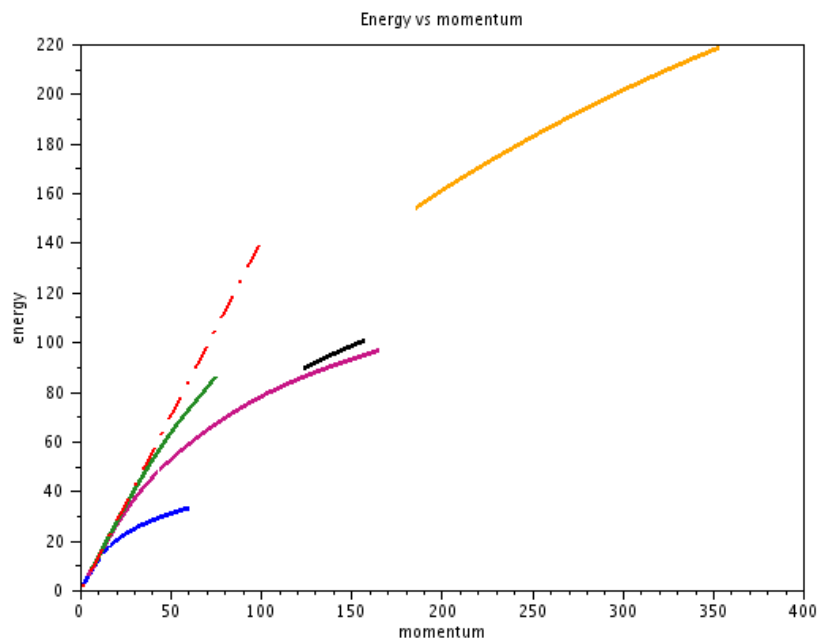


FIGURE 2. Energy-Momentum diagram with the multiple branches of 2D travelling waves of GP

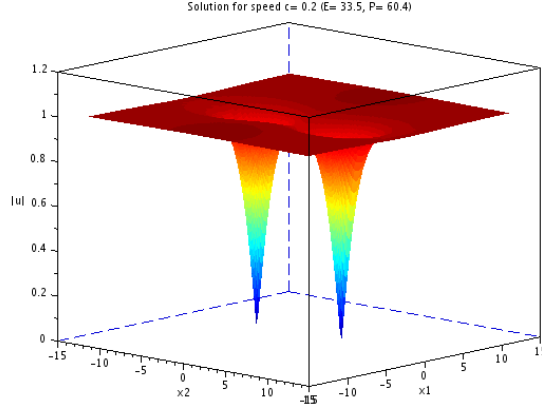


FIGURE 3. Travelling wave of the JR branch for $c = 0.2$ with two $(+1, -1)$ vortices ([21])

1.2. Vortex asymptotics $c \approx 0$.

A vortex is a particular stationary solution of the GP equation, see [18]. In polar coordinates it writes

$$V_n(x) = \mathbf{a}_n(r)e^{in\theta}, \quad (2)$$

with n a given nonzero integer called the *degree* of the vortex. The modulus \mathbf{a}_n solves the ODE

$$\mathbf{a}_n'' + \frac{\mathbf{a}_n'}{r} - \frac{n^2}{r^2}\mathbf{a}_n + \mathbf{a}_n(1 - \mathbf{a}_n^2) = 0, \quad (3)$$

with $\mathbf{a}_n(0) = 0$ and $\lim_{r \rightarrow +\infty} \mathbf{a}_n(r) = 1$. We refer to [32], [20], [9] for the analysis of (3).

Quite often, we call vortex any zero of the wave function, and it is expected that the wave function is close to some V_n near this zero. The vortex solution V_n is of infinite energy. However configurations involving several vortices (with possibly different degrees) could lead to finite energy solutions. At small speeds $c \rightarrow 0$, the travelling waves of the JR branch for the GP equation exhibit two vortices: the first one is of degree $+1$ and is located at z_1 and the second one is of degree -1 and is located at z_2 , with $z_1 = -z_2 \approx (0, 1)/c$, see figure 3 for a plot. A good approximation of this travelling wave is then given by

$$u_c(x) \approx V_1(x_1, x_2 - 1/c)V_{-1}(x_1, x_2 + 1/c). \quad (4)$$

The paper [8] provides a rigorous mathematical justification for the asymptotic limit $c \approx 0$ for the travelling waves of the JR branch.

Since the vortices are well separated when $c \rightarrow 0$, an asymptotic description by the Kirchhoff energy, very similar to what is known for classical incompressible fluids (see [23]), is possible. More precisely, assume that u is a wave function involving p vortices ($p \geq 2$), each one located at z_k and of degree n_k , in the sense that

$$u(x) \approx \prod_{k=1}^p V_{n_k}(x - z_k). \quad (5)$$

We assume that the vortices are well separated, that is $z_k = Z_k/c = c^{-1}(Z_{k,1}, Z_{k,2}) \in \mathbb{R}^2$, with the Z_k 's such that, as $c \rightarrow 0$, $|Z_k|$ are of order one and $|Z_k - Z_j|$ does not go to 0. We also assume that $\sum_{k=1}^p n_k = 0$, in

order to have finite energy. Then, [26] (see also [6]) shows the following asymptotic expansion

$$E(u) = 2\pi|\ln c| \sum_{k=1}^p n_k^2 + \sum_{k=1}^p \gamma(|n_k|) + \mathcal{E}(Z, \mathbf{n}) + o_{c \rightarrow 0}(1),$$

where $\gamma(|n|)$ is the core energy of the vortex of degree n , $\mathbf{n} = (n_1, \dots, n_p) \in \mathbb{Z}^p$ and where

$$\mathcal{E}(Z, \mathbf{n}) \stackrel{\text{def}}{=} -2\pi \sum_{j \neq k} n_j n_k \ln |Z_j - Z_k|$$

is the Kirchhoff interaction energy. The point vortex system obtained for the Euler incompressible equations, which is the Hamiltonian flow associated the Kirchhoff energy \mathcal{E} , may actually be derived for GP, see *e.g.*, [17], [26] and [6] for rigorous results.

For a wave function u with such well separated vortices, the asymptotics for the momentum has been given in [8]:

$$P(u) \approx \frac{2\pi}{c} \sum_{k=1}^p n_k Z_{k,2}.$$

As a consequence, the corresponding action for u is given by

$$E(u) - cP(u) = 2\pi|\ln c| \sum_{k=1}^p n_k^2 + \sum_{k=1}^p \gamma(|n_k|) + \mathcal{F}(Z, \mathbf{n}) + o_{c \rightarrow 0}(1),$$

where

$$\mathcal{F}(Z, \mathbf{n}) \stackrel{\text{def}}{=} -2\pi \sum_{j \neq k} n_j n_k \ln |Z_j - Z_k| - 2\pi \sum_{k=1}^p n_k Z_{k,2}.$$

Since the first two terms in the expansion of the action do not depend on the positions Z of the vortices, it is natural to think that if u is a travelling wave for GP with vortices as in (5), then (Z_1, \dots, Z_p) is a critical point of the reduced action \mathcal{F} , that is a solution to the nonlinear system

$$\forall k \in \llbracket 1, p \rrbracket, \quad 2 \sum_{\substack{1 \leq j \leq p \\ j \neq k}} n_j \frac{Z_j - Z_k}{|Z_j - Z_k|^2} = \begin{pmatrix} 0 \\ 1 \end{pmatrix}, \quad (6)$$

The proof that (6) is necessary may be found in [3] for the Ginzburg-Landau model (in a bounded domain and a Dirichlet boundary condition). If the travelling wave has two $(+1, -1)$ vortices (then $p = 2$) and, say $n_1 = 1$, $n_2 = -1$, and we do not loose generality assuming $Z_1 + Z_2 = 0$, which freezes the translation invariance. The equation (6) then reduces to

$$\frac{Z_1}{|Z_1|^2} = \begin{pmatrix} 0 \\ 1 \end{pmatrix},$$

and the solution is $Z_1 = (0, 1)$, which is the location of the vortices for the JR branch.

1.3. Transonic limit $c \approx \mathbf{c}_s$

As $c \rightarrow \mathbf{c}_s$, the travelling waves are expected to behave as rarefaction waves driven by the Kadomtsev-Petviashvili I (KP-I) equation. Following [21], [22], we introduce the following scalings:

$$\varepsilon = \sqrt{\mathbf{c}_s^2 - c^2}, \quad z_1 \stackrel{\text{def}}{=} \varepsilon x_1, \quad z_2 \stackrel{\text{def}}{=} \varepsilon^2 x_2, \quad (7)$$

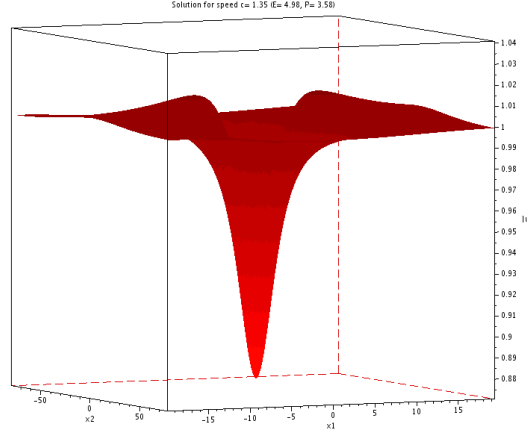


FIGURE 4. A rarefaction wave of the JR branch for $c = 1.35$ ([21])

and the ansatz

$$u(x) = \left(1 + \varepsilon^2 A_\varepsilon(z)\right) \exp(i\varepsilon\varphi_\varepsilon(z)), \quad (8)$$

where now, both φ_ε and A_ε tend to 0 at spatial infinity. Then, formal computations (see [21], [22]), assuming that $A_\varepsilon \rightarrow A$ and $\varphi_\varepsilon \rightarrow \varphi$ in some suitable sense as $\varepsilon \rightarrow 0$, that is $c \rightarrow \mathbf{c}_s$, show that A must be a solution to the solitary wave equation for the KP-I equation:

$$\partial_{z_1} A - \partial_{z_1}^3 A + 12A\partial_{z_1} A + 2\partial_{z_2}^2 \partial_{z_1}^{-1} A = 0 \quad (9)$$

and

$$\mathbf{c}_s A = \partial_{z_1} \varphi. \quad (10)$$

As $c \approx \mathbf{c}_s$ travelling waves are expected to behave (in the good scaling) as the Lump, expected to be the ground state. For mathematical results on the solitary waves of KP-I, see [15]. Complete justifications of the KP-I solitary wave limit for the travelling waves of GP have been given in [4] and in [12] (for a general nonlinearity and dimensions two and three). We refer to figure 4 for a plot of the travelling wave on the JR branch for $c = 1.35 \approx \sqrt{2}$.

1.4. Outline of the paper

As we have seen, the asymptotic behaviour $c \rightarrow 0$ and $c \rightarrow \mathbf{c}_s$ are well understood for the travelling waves of GP. The natural questions that arise are: if we know other solitary waves solutions to KP-I does this give branches of travelling waves for GP at least for $c \rightarrow \mathbf{c}_s$? and if we know some solution to (6), does this give branches of travelling waves for GP at least for $c \rightarrow 0$? We answer positively to these questions. Due to the integrability of KP-I (in 2D), explicit solitary waves have been given in [27], yielding for GP the purple and green branches in our Energy-Momentum diagram (figure 2). The black and the yellow branches are associated with other solutions to (6), namely the configuration $(-2, +2)$ located at $Z_1 = -Z_2 = (0, 2)$ and the configuration $(-2, +2)$ located at $Z_1 = -Z_2 = (0, 3)$. To the best knowledge of the authors, these questions have no theoretical answer yet, and have not been investigated numerically.

In order to compute these new travelling waves, we will have to design a numerical framework to approximate solutions of TW_c . Accordingly, section 2 will be dedicated to set up the needed numerical tools. The strategy follows closely [21] and [14]. Then, we will address in section 3 the question raised by the KP-I limit $c \rightarrow \mathbf{c}_s$.

We first describe the considered excited solitary waves given in [27]. Along the way, we wonder about their characteristics in the KP-I equation and propose to compute their numerical Morse index. We will thus consider the linearized KP-I equation for which we will compute the discrete eigenvalues within the numerical framework described in section 2. Finally, in section 4, we investigate the other vortex configurations $(+2, -2)$ and $(+3, -3)$.

2. NUMERICAL TOOLS

2.1. Discretization framework

First, we map \mathbb{R}^2 onto the square $\left[-\frac{\pi}{2}, \frac{\pi}{2}\right]^2$ using stretched coordinates as follows

$$R_1 x_1 = \tan(\hat{x}_1), \quad R_2 x_2 = \tan(\hat{x}_2), \quad (11)$$

where $(x_1, x_2) \in \mathbb{R}^2$, $(\hat{x}_1, \hat{x}_2) \in [-\pi/2, \pi/2]^2$, and R_1 and $R_2 > 0$ are adapted to the lengthscales of the solution we are interested in. This type of coordinates were used in [21] and we have used them in [14]. This mapping avoids working on an unbounded computational domain, hence the introduction of artificial boundary conditions. Another advantage of these stretched variables is that they allow to adapt to the typical lengthscales of the asymptotic regimes $c \approx 0$ or $c \approx c_s$. At the boundary of $\left[-\frac{\pi}{2}, \frac{\pi}{2}\right]^2$, we impose a Dirichlet boundary condition.

Any continuous problem is therefore first recast into this set of stretched variables and then solved numerically. The computational domain (i.e. the square $[-\pi/2, \pi/2]^2$) is discretized by a cartesian grid, with $N_{\hat{x}_1} \in \mathbb{N}^*$ points in the direction \hat{x}_1 and $N_{\hat{x}_2} \in \mathbb{N}^*$ points in the direction \hat{x}_2 . A uniform discretization (i.e. $N := N_{\hat{x}_1} = N_{\hat{x}_2}$) will be preferably chosen. We denote by h the size of the mesh (i.e. here $h = \pi/N$).

Each differential operator is expressed in the stretched coordinates (11) and then discretized within the Finite Difference framework. We refer to [14] for further details. Two types of discrete problems have to be considered. They are sketched in the two following subsections.

2.2. Discrete eigenvalue problems

First, we propose to compute the numerical Morse index of some explicit travelling wave solution of KP-I. Therefore we discretize the linearized KP-I differential operator around the corresponding solution. This leads to a discrete eigenvalue problem. More precisely, we have to solve a generalized eigenvalue problem of the following type

$$A_h u_h = \lambda_h B_h u_h, \quad (12)$$

with A_h and B_h two symmetric matrices. We refer the reader to subsection 3.1 for more details. We use the Scilab Software and its *eigs* function to compute the eigenvalues. The eigenvectors are computed using a classical power iteration algorithm.

2.3. Numerical travelling wave solutions

The second type of problem consists in computing, for a given speed $c > 0$, the numerical solution of TW_c . We emphasize the dependence of the solution u in speed c in the equation TW_c . This writes:

$$ic\partial_{x_1} u(c) - \Delta u(c) + u(c)(|u(c)|^2 - 1) = 0. \quad (13)$$

We shall impose the symmetries

$$u(x_1, x_2) = u(x_1, -x_2) = \bar{u}(-x_1, x_2). \quad (14)$$

Our goal is thus to compute the solution of (13), $u(c)$ at each speed c . To this end, we focus on continuation type methods. We will either work with Newton's method or a continuation method as in [16] and as recalled in the following subsection. The main principle is to start from a solution for speed c and use it to compute the solution at speed $c + \delta c$ for δc small.

2.3.1. Newton's method

We consider the continuous stretched formulation of (13) (i.e. in the system of coordinates (11)). Each stretched differential operator is discretized with finite differences. This induces the discrete nonlinear system for $u_{c,h}$ (the approximation of u_c):

$$\mathcal{T}_{c,h}(u_{c,h}) = 0. \quad (15)$$

Then the algorithm is simply:

- Initialization: $\varepsilon > 0$, $c_0 > 0$, $u_{c_0,h}$ given.
- Iteration: $u_{c,h}$ given, find $u_{c+\delta c,h}$ solution of $\mathcal{T}_{c+\delta c,h}(u_{c+\delta c,h}) = 0$ with Newton's algorithm.
 - (a) Initialization: $u^0 = u_{c,h}$,
 - (b) Iteration: Do $u^{k+1} = u^k - D\mathcal{T}_{c+\delta c,h}(u^k)^{-1} \cdot \mathcal{T}_{c+\delta c,h}(u^k)$, $k \leftarrow k + 1$, until $\frac{|\mathcal{T}_{c+\delta c,h}(u^k)|}{\|\partial_{x_1}^h u^k\|} \leq \varepsilon$,
 - (c) $k_{stop} := k$,
 - (d) $u_{c+\delta c,h} = u^{k_{stop}}$
- $c \leftarrow c + \delta c$

Newton's method has the advantage to be very efficient (when it converges) with a control over the residual of the equation (typically, in the computations, we achieve $\varepsilon = 10^{-8}$). However, Newton's method can require several iterations to converge (which in turn implies to solve the linear system several times in step (b)) and can also fail to compute a solution especially in the transonic limit. So that the recourse to another method is mandatory.

2.3.2. Continuation method

Inspired by [16], we formally differentiate (13) with respect to the speed c to obtain:

$$\Upsilon_c \left(\frac{\partial u}{\partial c}(c) \right) = i\partial_{x_1} u(c) \quad (16)$$

where

$$\Upsilon_c(v) \stackrel{\text{def}}{=} \Delta v - 2u(c)\langle u(c), v \rangle + (1 - |u(c)|^2)v - ic\partial_{x_1} v \quad (17)$$

is the linearized operator around $u(c)$. Equation (16) is viewed as an Ordinary Differential Equation determining $\frac{\partial u}{\partial c}$, provided we may invert Υ_c . We refer the reader to [14] for a discussion on this topic.

We compute the associated discrete operator $\Upsilon_{c,h}$ (associated to Υ_c) in the stretched variables using the Finite Difference framework proposed in subsection 2.1 and follow an iterative procedure.

- Initialization: $c_0 > 0$, $u_{c_0,h}$ given.
- Iteration: $u_{c,h}$ given, find $u_{c+\delta c,h}$ solution of (13).
 - (a) Compute $\partial_c^h u := \Upsilon_{c,h}^{-1}(i\partial_{x_1}^h u_{c,h})$ with $\partial_{x_1}^h$ the finite difference discretization of ∂_{x_1} in the stretched variables. This requires to solve one linear system.
 - (b) Update the solution to $u_{c+\delta c,h}$ for the speed $c + \delta c$, with $u_{c+\delta c,h} = u_{c,h} + \delta c \partial_c^h u$.
- $c \leftarrow c + \delta c$

At each step, one has to solve a linear system, and in the transonic limit, the latter can be hard to solve (see the discussion in section 3.5. of [14]). Contrary to Newton's method, step (a) requires only one system resolution, but we do not have any control on the residual. However even if we do not impose a control on this residual directly with the continuation method, it allows, with a good initial residual (*i.e.* at the beginning of the iteration procedure), to compute an accurate solution everywhere and especially in regions where Newton's method may fail to converge. Since this numerical strategy has already been studied and validated in [14], we choose not to give extensive details and refer the reader to the latter reference.

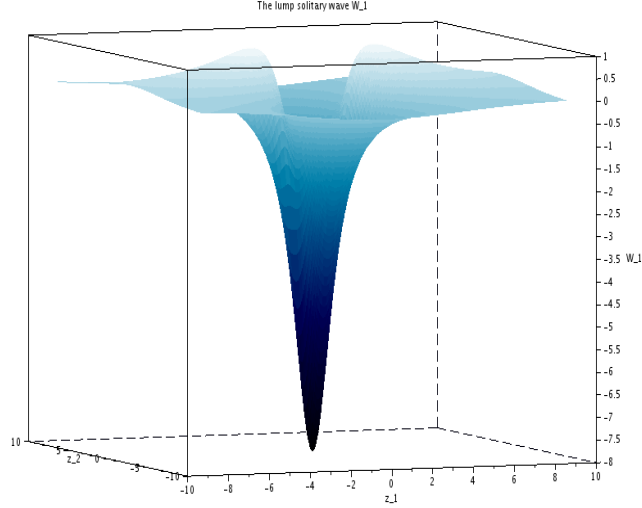


FIGURE 5. Representation of the first Lump solitary wave \mathcal{W}_1 of KP-I.

3. OTHER BRANCHES OF TRAVELLING WAVE SOLUTIONS TO GP WITH KP-I ASYMPTOTICS

3.1. Explicit solitary waves solutions to KP-I and their numerical Morse index

3.1.1. *Explicit solitary wave solutions to KP-I*

We focus on the adimensionalized version of the solitary wave equation for KP-I given in (9):

$$\partial_{z_1} \mathcal{W} - \partial_{z_1}^3 \mathcal{W} + \mathcal{W} \partial_{z_1} \mathcal{W} + \partial_{z_2}^2 \partial_{z_1}^{-1} \mathcal{W} = 0. \quad (\text{SW})$$

from which A (as defined in section 1.3) is recovered through the scaling

$$A(z_1, z_2) = \frac{1}{12} \mathcal{W}\left(z_1, \frac{z_2}{\sqrt{2}}\right). \quad (18)$$

We know that equation SW is integrable in 2D and that there exist explicit solutions. The first and well known one is the Lump solitary wave found in [24]. Its explicit expression is given as a z_1 -derivative of a rational function as follows:

$$\mathcal{W}_1(z) = -12 \partial_{z_1}^2 \ln(3 + z_1^2 + z_2^2) = -24 \frac{3 - z_1^2 + z_2^2}{(3 + z_1^2 + z_2^2)^2}. \quad (19)$$

This solution is expected to be the ground state of SW, though, to the best knowledge of the authors, no proof is available. See figure 5 for a graphical representation. The rarefaction wave of the JR branch of travelling waves for GP plotted in figure 4 is clearly related to the \mathcal{W}_1 lump through the ansatz (8) and the scaling (7).

Furthermore, other explicit solutions to this equation have been obtained by the Hirota method in [27]. The expression of the second Lump solution is given by

$$\mathcal{W}_2(z) = 12 \partial_{z_1}^2 \ln((z_1^2 + z_2^2)^3 + 25z_1^4 + 90z_1^2 z_2^2 + 17z_2^4 + 475z_2^2 + 1875). \quad (20)$$

See figure 6 for a graphical representation. The third lump is given by

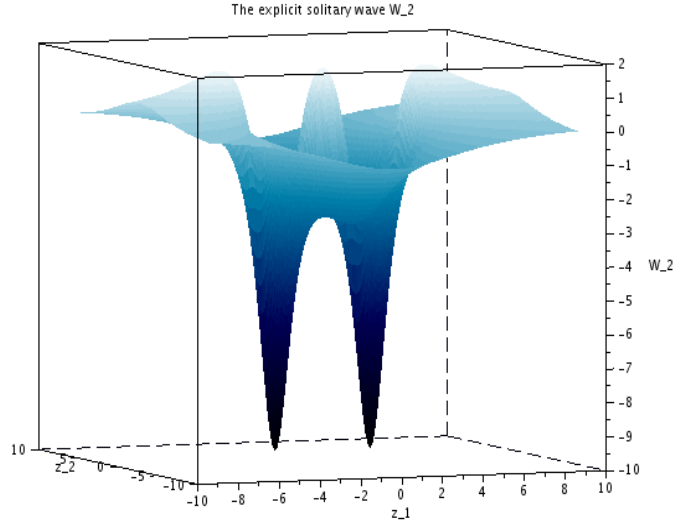


FIGURE 6. Representation of the second Lump solitary wave \mathcal{W}_2 of KP-I.

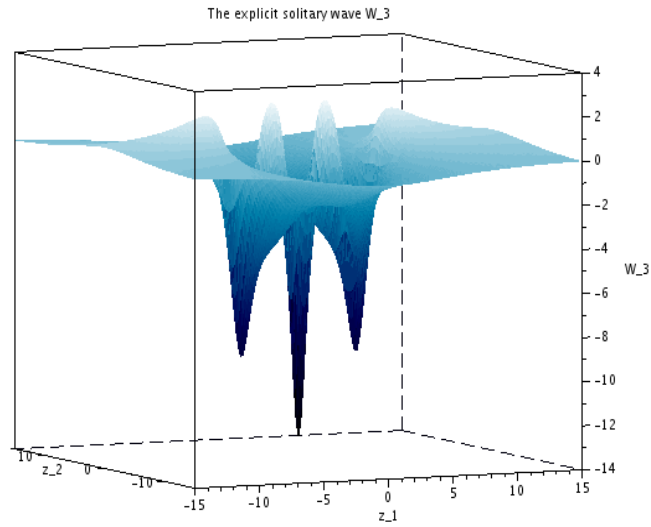


FIGURE 7. Representation of the third Lump solitary wave \mathcal{W}_3 of KP-I.

$$\mathcal{W}_3(z) = 12\partial_{z_1}^2 \ln \left((z_1^2 + z_2^2)^6 + \dots + \frac{159786550}{3}z_1^2 + \dots + \frac{878826025}{9} \right). \quad (21)$$

See figure 7 for a graphical representation.

The reader may notice the increasing degree of the polynomial appearing in the expressions, that makes the computations harder and harder but theoretically feasible. One is expecting explicit solutions of higher "degrees" by continuing the arguments and computations of [27].

On the mathematical level, the only result the authors know about multiplicity results for solitary waves to the generalized KP-I equation (with nonlinearity $\mathcal{W}\partial_{z_1}f(\mathcal{W})$) is the paper [31], where the existence of at least two solitary waves is shown with the help of Lusternik-Schnirelman category.

Before concentrating on the possible branches of travelling waves solutions associated with these explicit KP-I solitary waves, we propose to study some of the properties of the latter through the computation of their numerical Morse index.

3.1.2. Numerical Morse Index

In order to compute the Morse index associated to each explicit solitary wave, we study the linearized operator around each explicit solution. The formal linearization of the SW equation around one explicit solution \mathcal{W} gives the operator \mathcal{L} :

$$\mathcal{L}(w) \stackrel{\text{def}}{=} w - \partial_{z_1}^2 w + \mathcal{W}w + \partial_{z_2}^2 \partial_{z_1}^{-2} w. \quad (22)$$

The eigenvalue problem then reads

$$\mathcal{L}(w) = \lambda w. \quad (23)$$

In order to get rid of the non local term $\partial_{z_1}^{-2} w$, let us suppose that w writes as

$$w = \partial_{z_1} \Theta.$$

To stick with a variational formulation we then apply the operator ∂_{z_1} to the equation (23). This gives, denoting

$$\mathcal{L}_1(\Theta) \stackrel{\text{def}}{=} -\partial_{z_1}^2 \Theta + \partial_{z_1}^4 \Theta - \partial_{z_1}(\mathcal{W}\partial_{z_1} \Theta) - \partial_{z_2}^2 \Theta, \quad (24)$$

the following eigenvalue problem

$$\mathcal{L}_1(\Theta) = -\lambda \partial_{z_1}^2 \Theta. \quad (25)$$

The latter has a variational formulation, that is \mathcal{L}_1 and $\partial_{z_1}^2$ are formally self-adjoint.

Furthermore, clearly, $w_1 \stackrel{\text{def}}{=} \partial_{z_1} \mathcal{W}$ and $w_2 \stackrel{\text{def}}{=} \partial_{z_2} \mathcal{W}$ belong to $\ker(\mathcal{L})$, which means that for the lump \mathcal{W}_1 for instance,

$$\Theta_{1,1} \stackrel{\text{def}}{=} -24 \frac{z_1}{3 + z_1^2 + z_2^2}$$

and

$$\Theta_{1,2} \stackrel{\text{def}}{=} 48 \frac{z_1 z_2}{(3 + z_1^2 + z_2^2)^2}.$$

belong to $\ker(\mathcal{L}_1)$. However, notice that in section 2.3, we impose the symmetries (14), so that the linear operators used in the algorithms are invertible. In the sequel, we concentrate on the eigenvalue problem (25) on the whole \mathbb{R}^2 without symmetry to characterize each explicit Lump solutions.

We follow the strategy of discretization explicited in section 2. In other words, we recast the continuous equations in the set of stretched variables. Doing so, the variational structure of the equations is kept in a weighted L^2 space. We wish to preserve the symmetry of the variational operators. In the discrete setting, we then use classical centered finite difference formula and discrete integration by parts.

We are thus led to the discrete generalized eigenvalue problem that corresponds to the discrete version of (25): *Find* (λ_h, v_h) *such that*

$$A_h v_h = \lambda_h B_h v_h, \quad (26)$$

with A_h and B_h two symmetric matrices.

We present in table 1 some of the eigenvalues we obtain (from the smaller ones) for the first three Lump solitary waves presented in this work. For each case, we clearly distinguish between negative eigenvalues (in red) and zero eigenvalues (with multiplicity, in blue) and positive ones (in black). As a consequence, we argue that

\mathcal{W}_1	\mathcal{W}_2	\mathcal{W}_3
-2.3581	-3.5882	-4.5854
-0.0076	-2.5773	-3.4559
-0.0049	-0.8462	-2.6317
0.6737	-0.3303	-1.3209
0.8617	- 0.0177	-1.1986
	- 0.0104	-0.7652
	- 0.0047	-0.4805
	- 0.0011	-0.3876
	0.2625	-0.2253
	0.4544	- 0.0309
	0.5840	- 0.0186
		- 0.0163
		- 0.0091
		- 0.0076
		- 0.0016
		0.1612
		0.2817
		0.3322

TABLE 1. First numerical eigenvalues for the first three lump solitary waves.

Lump solitary wave	Numerical Morse index
\mathcal{W}_1	1
\mathcal{W}_2	4
\mathcal{W}_3	9

TABLE 2. Computation of the numerical Morse index.

the numerical Morse index for the first three lump solitary waves are as in table 2. One example of a typical eigenvector is shown in Figure 8. We find a Morse index of 1 for the first Lump \mathcal{W}_1 , as expected if it is indeed a/the ground state for KP-I and then minimizes the energy at fixed momentum. From the above results, it is natural to *conjecture* that *the Morse index of the n -th Lump solitary wave \mathcal{W}_n is n^2 .*

Let us now concentrate on the Kernel. We plotted the eigenvector for \mathcal{W}_1 corresponding to the eigenvalue -0.0076 and -0.0049 . We verified that they are identified (as expected) to $\Theta_{1,1}$ and $\Theta_{1,2}$. However, we point out that its determination is quite challenging, since we have to deal with the fact that the essential spectrum of \mathcal{L}_1 is \mathbb{R}^+ . Despite this fact, we conjecture that: *the n -th Lump solitary wave \mathcal{W}_n has a Kernel of dimension $2n$.*

We now continue with the study of multiple branches of travelling wave solution issued from the explicit KP-I solitary waves.

3.2. The Energy-Momentum diagram for GP in 2D: the JR branch

We begin with the well known case of the JR branch of travelling waves obtained in [21], for which the Energy-Momentum diagram is given in Figure 1. This branch is characterized by two vortices for $c \approx 0$ and by the KP-I asymptotic limit associated with the \mathcal{W}_1 Lump solitary wave when $c \approx \mathbf{c}_s$. Actually, one may obtain numerically this branch starting either from $c \approx \mathbf{c}_s$ and an approximate solution given by (8)-(10) with

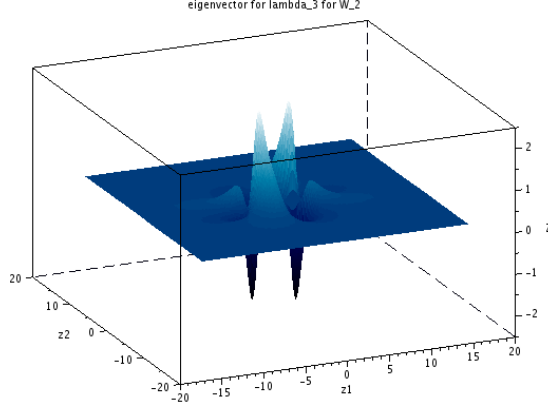


FIGURE 8. Representation of the third eigenvector corresponding to the third negative eigenvalue ($\lambda_3 = -0.846$) of the second Lump \mathcal{W}_2 .

A related to the Lump solitary wave \mathcal{W}_1 through (18), either from $c \approx 0$ and an approximate solution given by (4), provided we have an approximation of the vortex profile \mathbf{a}_1 (see subsection 4.1). For details, we refer the reader to [21] and [14]. We give two types of representations of the travelling waves solutions on the JR branch. In figure 9, we plot, for various speeds c , on the right-hand side, the 3d plot of the modulus of the travelling wave in the domain $\{x_1 \geq 0\}$ (in the domain $\{x_1 \leq 0\}$, it suffices to use the symmetry (14)) and on the left-hand side the corresponding position on the Energy-Momentum diagram. Figure 10 contains contour plot views on the whole plane \mathbb{R}^2 . One clearly sees the evolution as the speed of the wave increases: for $c \approx 0$, we have two well-separated vortices at distance $\approx 1/c$ one from another; they get closer when c increases and at some step merge, and for higher speeds, vorticity is lost; for $c \approx c_s$, the modulus is uniformly close to 1 and the travelling wave is a rarefaction pulse as in figure 4.

On the numerical level, two approaches can be used to obtain this branch. The first one, used in [21], is based on Newton's algorithm (see subsection 2.3); the other one is based on the variational properties of the problem and looks for finding (local) minimizers to suitable functionals (*cf.* [14]). The local minimizing technique has many advantages over a continuation method; it is quick, systematic (relying on a heat flow technique) and precise (see [14] for details). However, to try to catch numerically the other possible branches of solutions arising from the second and third Lump as described in section 3.1, we can not rely on such a minimization procedure. Therefore, we focus on continuation type methods as described in subsection 2.3.

3.3. New branch of travelling waves associated with the second lump \mathcal{W}_2 .

Let us concentrate on the second Lump \mathcal{W}_2 , that has the expression (20). We use the scalings (7) and initialize a continuation method with $c \approx c_s$ via the ansatz (8)-(10) and employing (20).

We plot the resulting Energy-Momentum diagram in Figure 11. The blue curve is the JR branch with the transonic limit given by the \mathcal{W}_1 Lump (see subsection 3.2). The purple curve represents the Energy-Momentum diagram obtained starting from the KP-I limit with the second Lump \mathcal{W}_2 .

Figures 12 and 13 depict the evolution of the modulus of the numerical travelling wave solution for various (decreasing) speeds. In figure 14, we give the corresponding contourplots. Similarly to the ground state branch, the minimum value of the modulus of the solution decreases until vortices appear by pairs. For $c = 0.73$, we see four vortices, and for c further decreasing, the local minimum of the modulus on the x_2 axis decreases down to zero and then two additional vortices appear: we end-up with six distinguishable vortices.

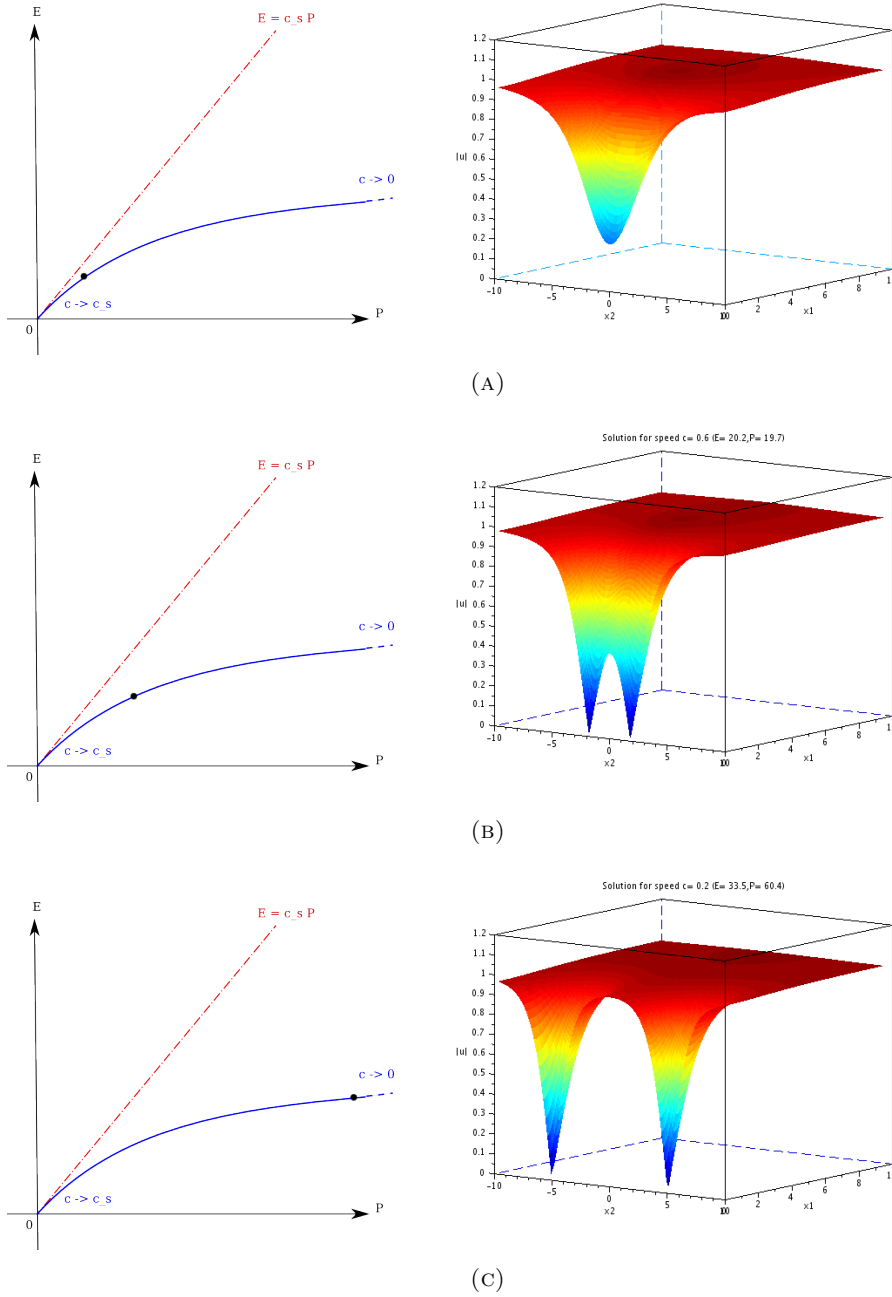


FIGURE 9. Travelling wave solution of the JR branch for speeds: (A) $c = 1$; (B) $c = 0.6$; (C) $c = 0.2$. On the left-hand side, position in the Energy-Momentum diagram (spotted with a black point); on the right-hand side, modulus.

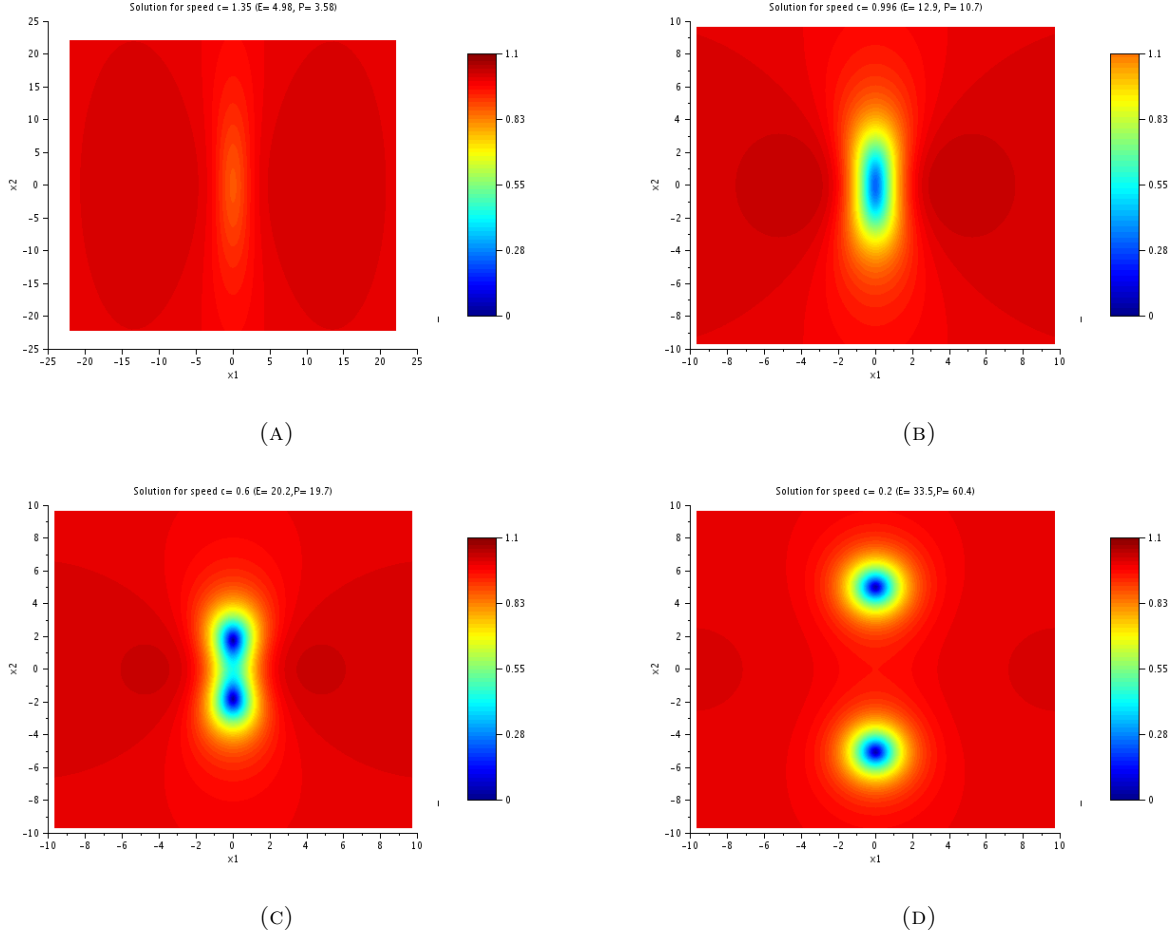


FIGURE 10. Contourplots of the travelling waves of the JR branch: (A) $c = 1.35$; (B) $c = 1$; (C) $c = 0.6$; (D) $c = 0.2$.

3.4. New branch of travelling waves associated with the third lump \mathcal{W}_3 .

We now turn to the third Lump solitary wave \mathcal{W}_3 given by (21). Analogously, we make use of (7) and initialize the continuation with $c \approx c_s$ via the ansatz (8). We plot the resulting Energy-Momentum diagram in Figure 15.

We obtain a third branch of travelling waves solutions. Figures 16 and 17 describe the evolution of the modulus of the computed travelling wave solution that we compute. In a similar fashion, the modulus of the minimum and local minima decrease as the speed decreases down to the speed ≈ 0.9 (see Figure 17 (A)). There vortices appear and we observe the same kind of splitting phenomenon as for the branch associated with the second Lump. At speed ≈ 0.685 , ten vortices are clearly distinguishable.

3.5. Conclusion

Our numerical simulation put forward two new branches of travelling wave solutions corresponding to excited states; these branches are distinct from the JR state branch and from each other. As can be checked in figures 10 (D), 14 (F) and 18 (F), we can conjecture that the branch associated with the n -th Lump solitary wave \mathcal{W}_n

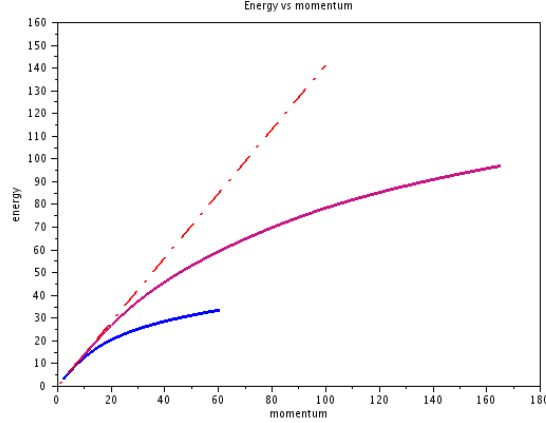


FIGURE 11. Energy-Momentum diagram with the JR branch (blue) and the new branch associated with the second Lump \mathcal{W}_2 (purple).

eventually exhibits $2(2n - 1)$ vortices. For the branch \mathcal{W}_2 (resp. \mathcal{W}_3), we have been able to reach the speed 0.27 (resp. 0.685). Below these speeds, our algorithms stop converging.

4. VORTEX BRANCHES

As motivated in subsection 1.4, we wonder whether $(+2, -2)$ and $(+3, -3)$ vortex configuration would generate a new branch of travelling waves solutions to GP or even connect to the branches obtained in the previous section. These configurations can be designed and used as initializations in our algorithm for $c \approx 0$.

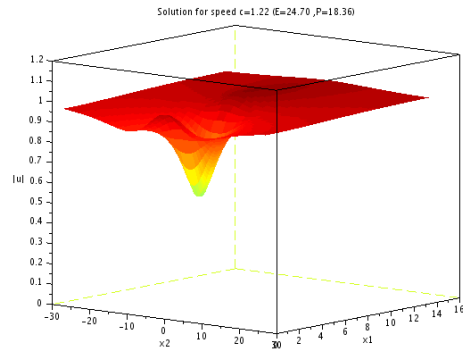
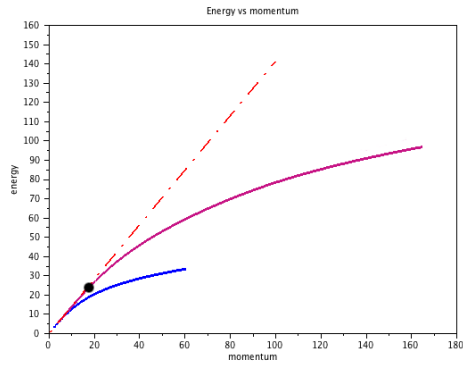
4.1. Approximating the vortices

The strategy adopted in this work consists in first finding a Padé approximant for the vortex profile of degree n , \mathbf{a}_n (see section 1.2 for notations), with here $n \in \{1, 2, 3\}$ from which one would create the "two vortices" configuration. A shooting method allows to compute an approximate numerical solution to (3) that will serve as a reference solution, denoted $\mathbf{a}_n^{\text{ref}}$. For this problem, in order to avoid the singularities of the ODE (3), it is convenient to implement the shooting method on the function $r \mapsto \mathbf{a}_n(r)/r^n$. Indeed, from [20], we know that $y_n(r) \stackrel{\text{def}}{=} \mathbf{a}_n(r)/r^n$ is an even power series of positive radius. The shooting parameter is then $y_n(0)$ and we have $y_n'(0) = 0$. For $n = 1$, we obtain $y_1(0) = \mathbf{a}_1^{\text{ref}'(0)} \approx 0.58318949586$, which is slightly different from the value ≈ 0.5827811878 in [2].

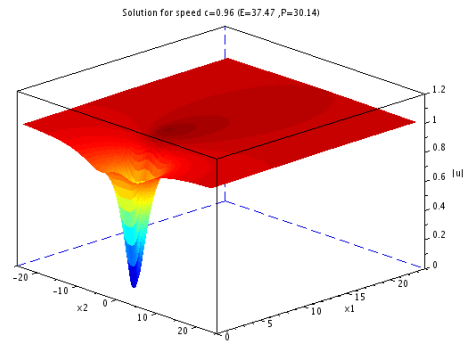
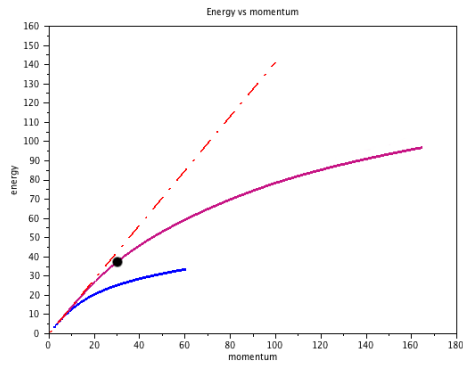
Here we envisage two strategies for computing the Padé approximants. The first one is taken from [2] and consists in looking for a Padé of the form

$$\mathbf{a}_1^{\text{Padé}}(r) \stackrel{\text{def}}{=} r \sqrt{\frac{a_0 + a_1 r^2}{1 + b_1 r^2 + b_2 r^4}}. \quad (27)$$

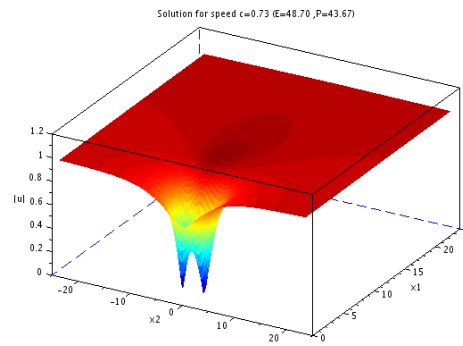
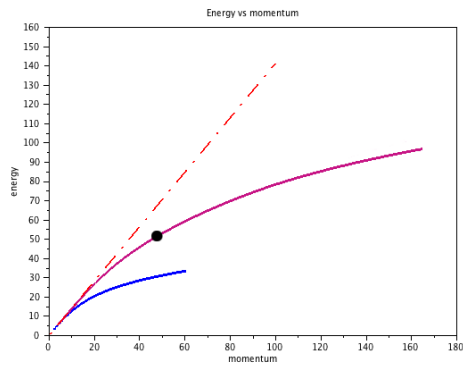
Since $\mathbf{a}_1(r) \rightarrow 1$ for $r \rightarrow +\infty$, it is natural to set $b_2 = a_1$. To determine the other coefficients, we substitute $\mathbf{a}_1^{\text{Padé}}$ in the equation (3) and Taylor expand the residual for $r \rightarrow 0$. We obtain three algebraic equations by cancelling the first coefficients of this Taylor expansion, and solve this system. We will refer to this method as



(A)

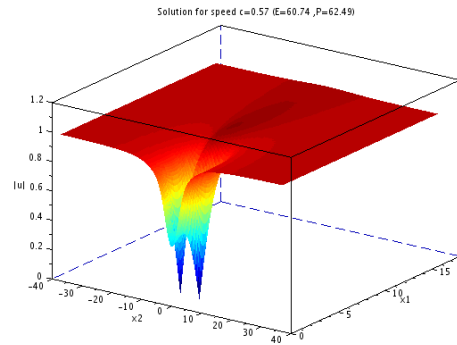
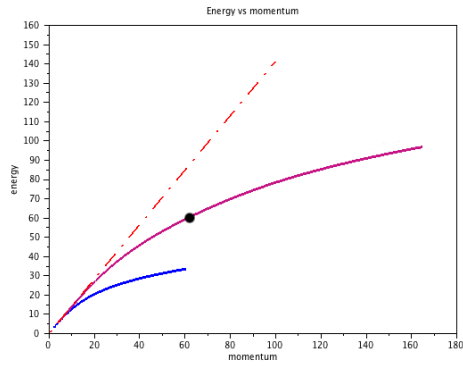


(B)

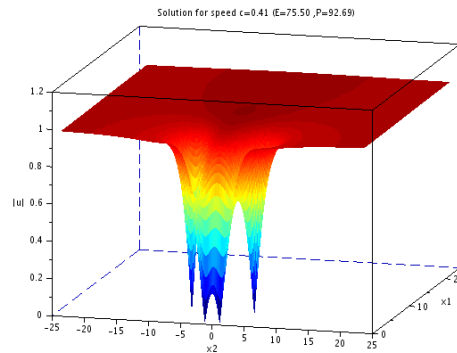
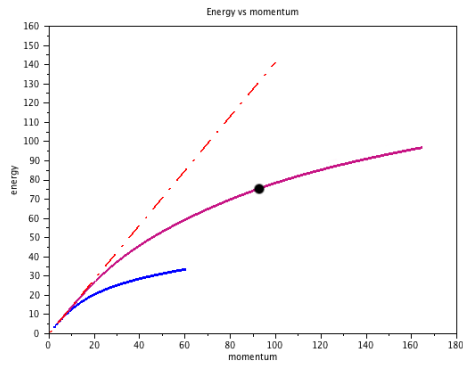


(C)

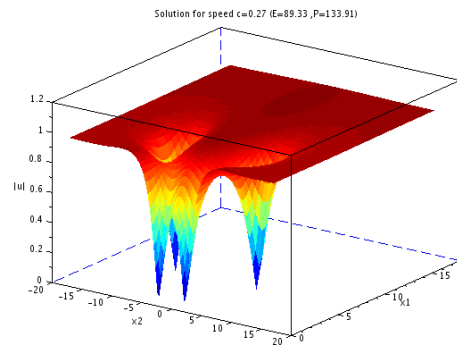
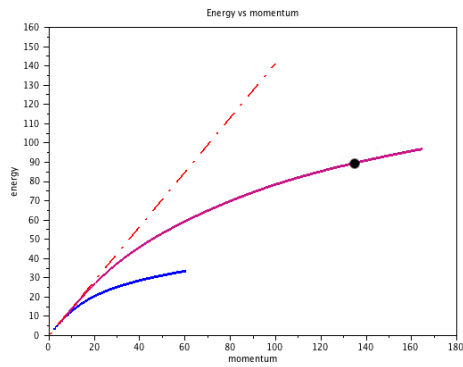
FIGURE 12. Travelling wave solution of the branch associated with the second Lump \mathcal{W}_2 for speeds: (A) $c = 1.22$; (B) $c = 0.96$; (C) $c = 0.73$. On the left-hand side, position in the Energy-Momentum diagram (spotted with a black point); on the right-hand side, modulus.



(A)



(B)



(C)

FIGURE 13. Travelling wave solution of the branch associated with the second Lump \mathcal{W}_2 for speeds: (A) $c = 0.57$; (B) $c = 0.41$; (C) $c = 0.27$. On the left-hand side, position in the Energy-Momentum diagram (spotted with a black point); on the right-hand side, modulus.

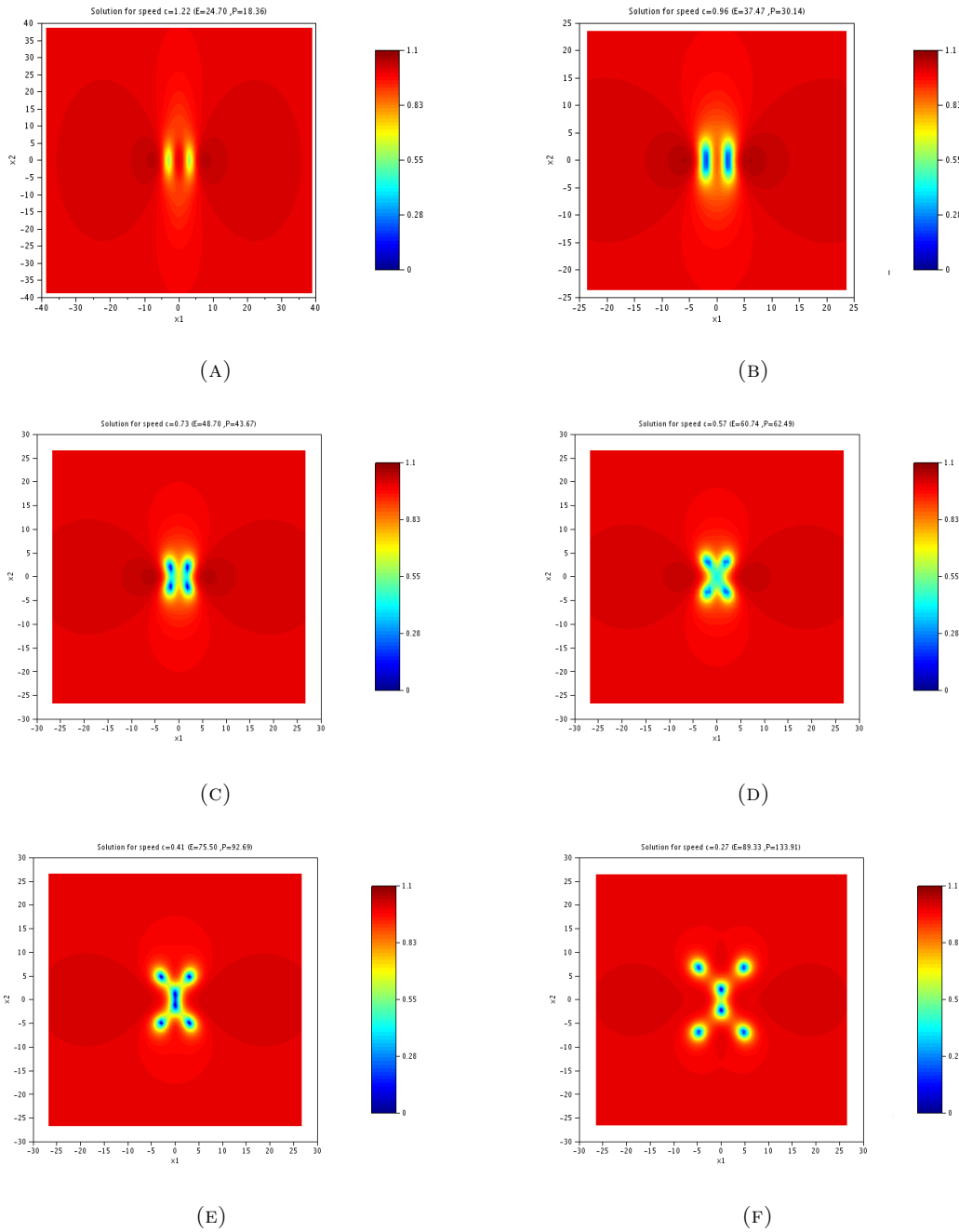


FIGURE 14. Contourplots of the travelling waves of the branch associated with the \mathcal{W}_2 Lump: (A) $c = 1.22$; (B) $c = 0.96$; (C) $c = 0.73$; (D) $c = 0.57$; (E) $c = 0.411$; (F) $c = 0.27$.

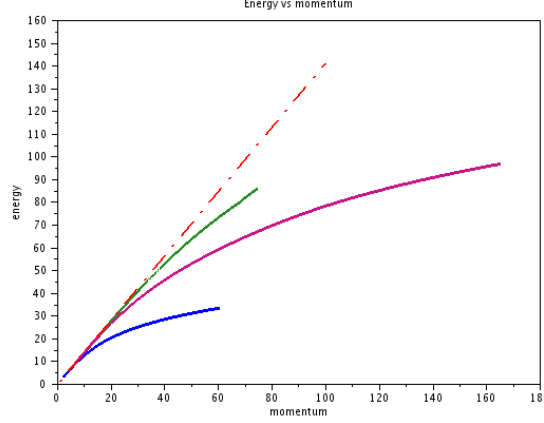


FIGURE 15. Energy-Momentum diagram with the JR branch (blue), the branch associated with the second lump \mathcal{W}_2 (purple) and with the third Lump \mathcal{W}_3 (green).

	<i>Berloff's</i>	<i>Least square</i>
L^2 error	0.0250530	0.0028370
L^∞ error	0.0097847	0.0013490

TABLE 3. Vortex of degree 1: L^2 and L^∞ errors between the Padé approximants and the numerical solution obtained with the shooting method.

Berloff's method, and this gives

$$\mathbf{a}_1^{\text{Be}}(r) \stackrel{\text{def}}{=} r \sqrt{\frac{\frac{11}{32} + \frac{11}{384}r^2}{1 + \frac{1}{3}r^2 + \frac{11}{384}r^4}} = r \sqrt{\frac{0.3437 + 0.0286r^2}{1 + 0.3333r^2 + 0.0286r^4}}. \quad (28)$$

The advantage of this method is that we do not need to solve numerically the ODE (3) by a shooting method. The second method, referred to as the *least square method*, consist in fitting a Padé approximant to the numerical data given by the numerical solution $\mathbf{a}_1^{\text{ref}}$ obtained by the shooting method. In order to do so, we use a least square method and obtain

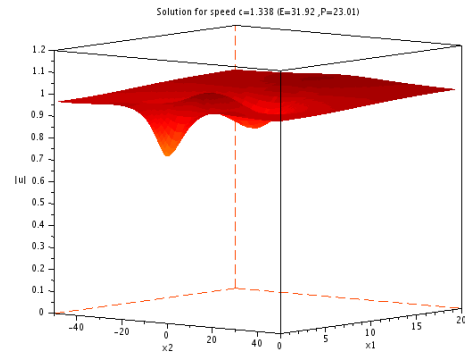
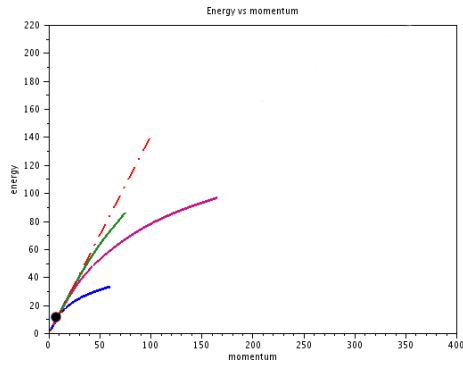
$$\mathbf{a}_1^{\text{ls}}(r) \stackrel{\text{def}}{=} r \sqrt{\frac{0.3350601 + 0.0494196r^2}{1 + 0.3725704r^2 + 0.0494196r^4}}. \quad (29)$$

We may notice that $\mathbf{a}_1(r)/r \rightarrow 0.58318949586$ when $r \rightarrow 0$. This has to be compared with $\sqrt{11/32} \approx 0.5863020$ and $\sqrt{0.3350601} \approx 0.5788438$. We may also compute the L^2 and L^∞ errors between \mathbf{a}_1^{Be} (resp. \mathbf{a}_1^{ls}) and $\mathbf{a}_1^{\text{ref}}$ (see table 3). We see that \mathbf{a}_1^{Be} gives a very good approximation, and that \mathbf{a}_1^{ls} provides an excellent approximation.

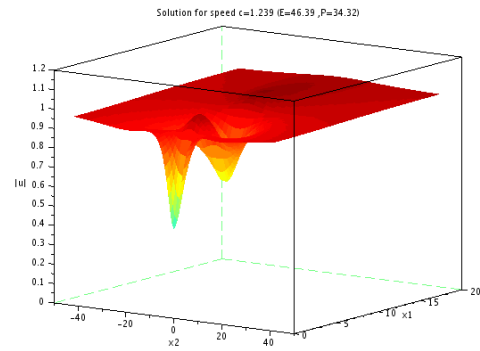
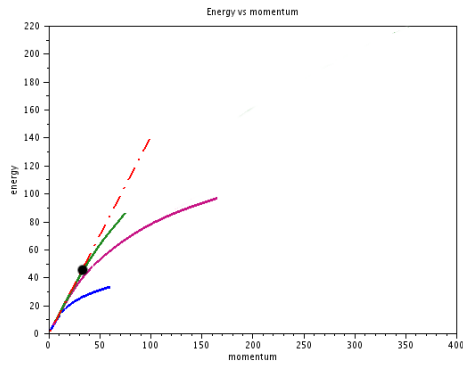
We now focus on the degrees 2 and 3 that have not yet been addressed.

4.1.1. Vortex of degree 2

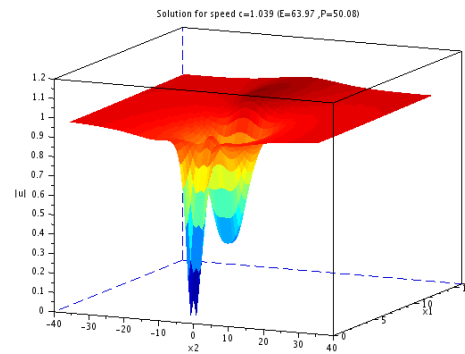
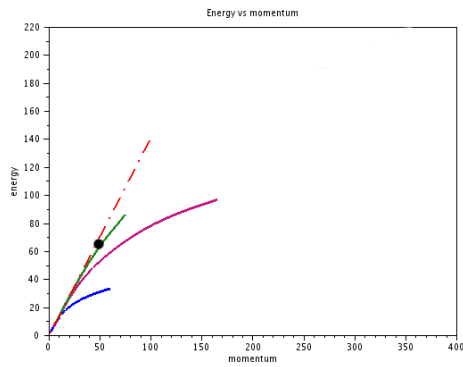
The solution obtained by the shooting method gives the approximate limit $r^{-2}\mathbf{a}_2^{\text{ref}}(r) \rightarrow 0.153099102859$ when $r \rightarrow 0$. In [2], the coefficients of the Padé approximant have been computed (with *Berloff's method*) and



(A)

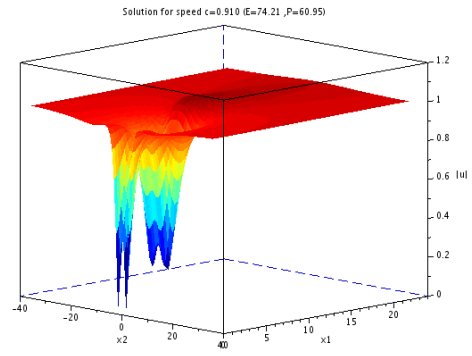
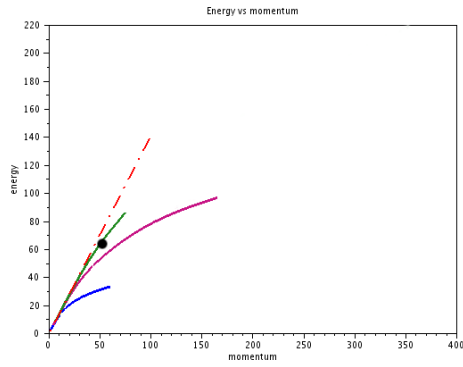


(B)

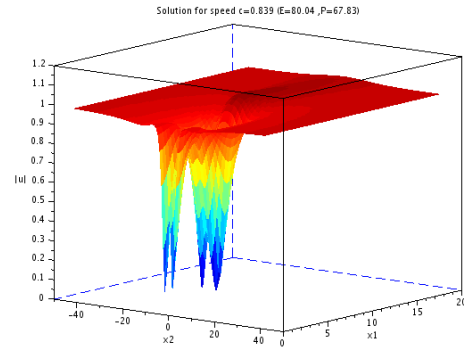
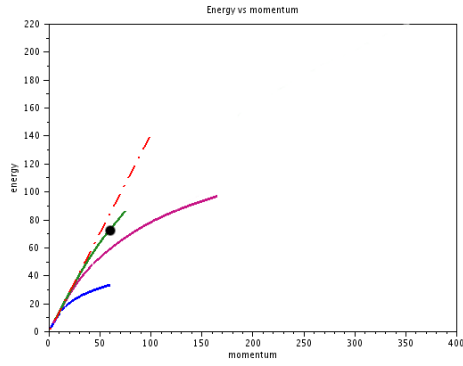


(C)

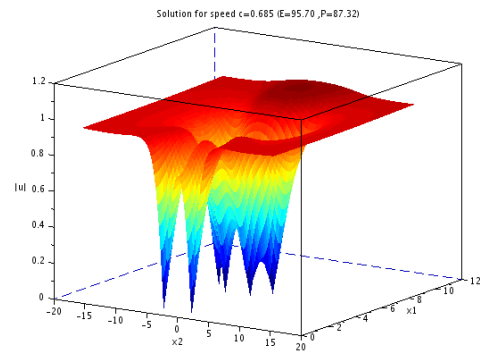
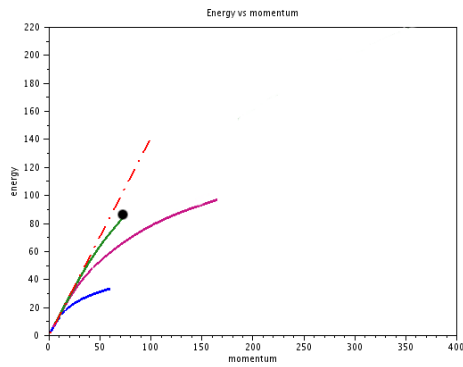
FIGURE 16. Travelling wave solution of the branch associated with the second Lump \mathcal{W}_3 for speeds: (A) $c = 1.34$; (B) $c = 1.24$; (C) $c = 1.04$. On the left-hand side, position in the Energy-Momentum diagram (spotted with a black point); on the right-hand side, modulus.



(A)



(B)



(C)

FIGURE 17. Travelling wave solution of the branch associated with the second Lump \mathcal{W}_3 for speeds: (A) $c = 0.91$; (B) $c = 0.84$; (C) $c = 0.685$. On the left-hand side, position in the Energy-Momentum diagram (spotted with a black point); on the right-hand side, modulus.

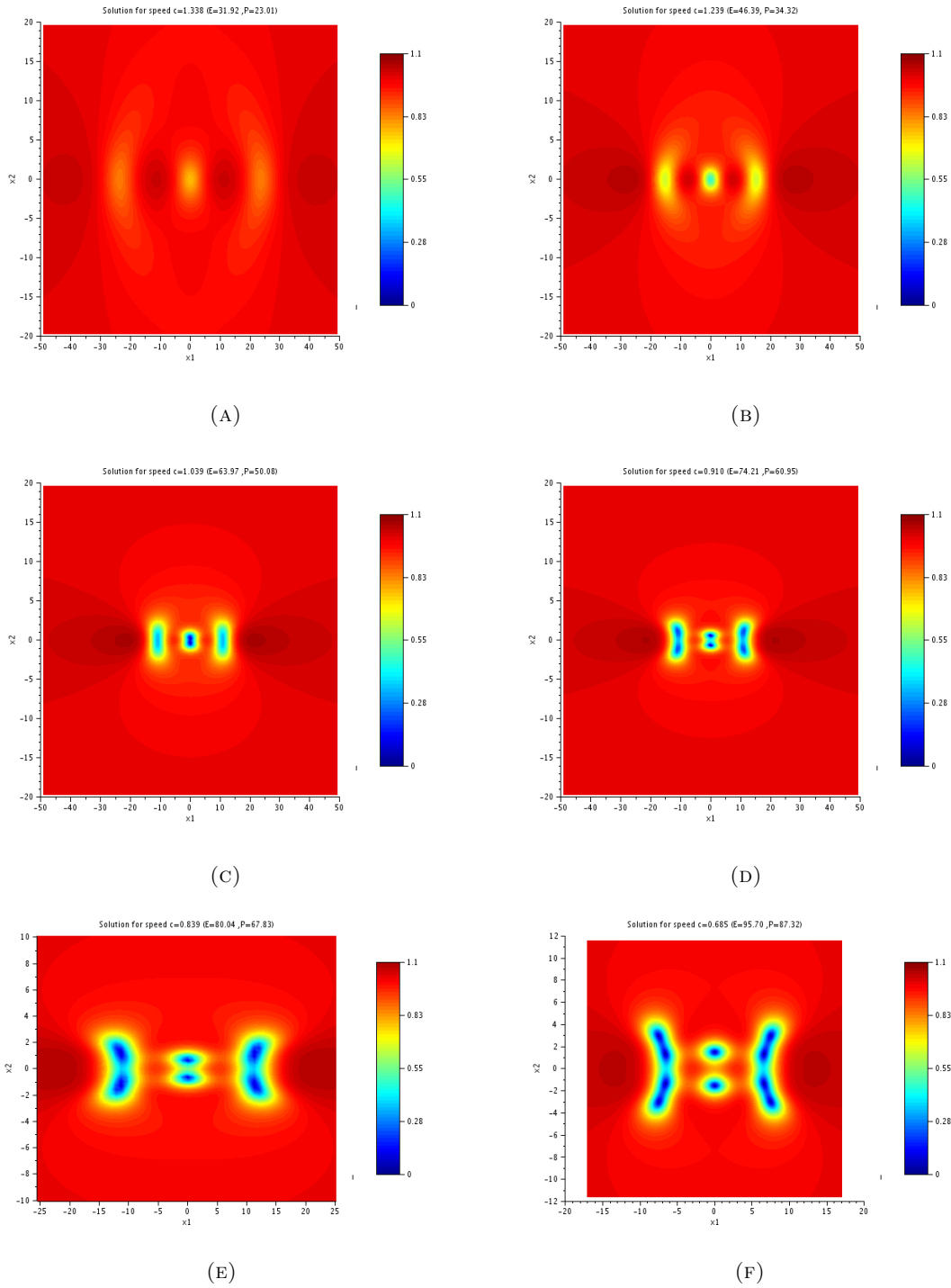


FIGURE 18. Contourplots of the travelling waves of the branch associated with the \mathcal{W}_3 Lump: (A) $c = 1.34$; (B) $c = 1.24$; (C) $c = 1.04$; (D) $c = 0.91$; (E) $c = 0.84$; (F) $c = 0.685$.

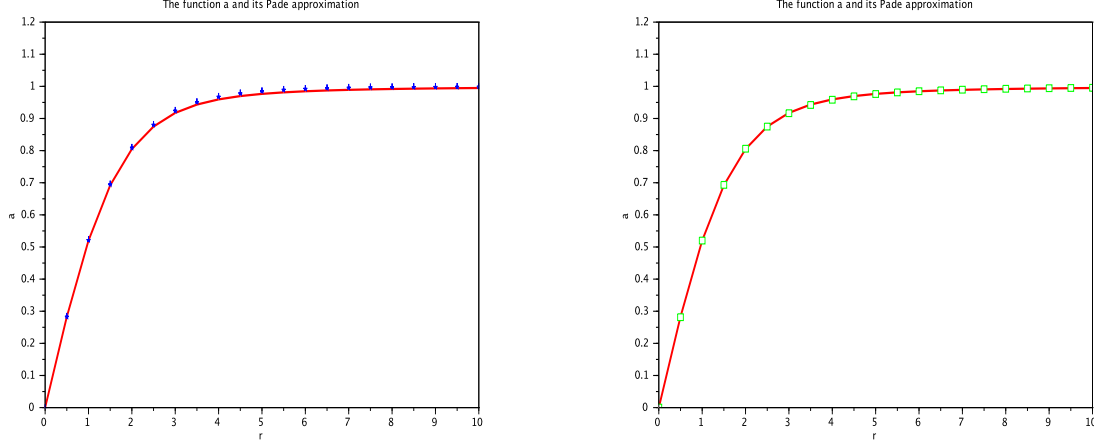


FIGURE 19. Profile of the degree 1 vortex \mathbf{a}_1 (continuous red line) and Padé approximants: \mathbf{a}_1^{Be} (28) in blue stars (left) and \mathbf{a}_1^{ls} (29) in green squares (right)

	<i>Berloff's</i>	<i>Least square</i>
L^2 error	0.1721167	0.0066131
L^∞ error	0.0619714	0.0084585

TABLE 4. Vortex of degree 2: L^2 and L^∞ errors between the Padé approximants and the numerical solution obtained with the shooting method.

give the expression

$$\mathbf{a}_2^{\text{Be}}(r) \stackrel{\text{def}}{=} r^2 \sqrt{\frac{0.02564396012 + 0.000626418393r^2}{1 + 0.1910941884r^2 + 0.01969625361r^4 + 0.000626418393r^6}} \quad (30)$$

that yields $r^{-2}\mathbf{a}_2^{\text{Be}}(r) \rightarrow \sqrt{0.02564396012} \approx 0.160137316$. Using the *least square method*, we obtain

$$\mathbf{a}_2^{\text{ls}}(r) \stackrel{\text{def}}{=} r^2 \sqrt{\frac{0.0208654 + 0.0010475r^2}{1 + 0.1504765r^2 + 0.0243630r^4 + 0.0010475r^6}}, \quad (31)$$

that gives the asymptotics $r^{-2}\mathbf{a}_2^{\text{ls}}(r) \rightarrow \sqrt{0.0208654} \approx 0.1444486$. In figure 20, we plot $\mathbf{a}_2^{\text{ref}}$, \mathbf{a}_2^{Be} , \mathbf{a}_2^{ls} . We also measure the L^2 and L^∞ errors between \mathbf{a}_2^{Be} (resp. \mathbf{a}_2^{ls}) and $\mathbf{a}_2^{\text{ref}}$ (see table 4). We notice a much better fit if one uses the least square method. Notice for instance that \mathbf{a}_2^{Be} reaches values larger than 1.

In order to improve the quality of the Padé approximation, one could imagine to consider a higher degree Padé approximant, namely, for our problem, replacing in the square root the rational function by the quotient of a polynomial of degree 4 by a polynomial of degree 8. With *Berloff's method*, we obtain the following expression for the Padé approximant of the vortex of degree 2 :

$$\mathbf{a}_{2\text{bis}}^{\text{Be}}(r) \stackrel{\text{def}}{=} r^2 \sqrt{\frac{0.0235754388705356 + 0.001903033787r^2 + 0.00007439596524r^4}{1 + 0.2473877000r^2 + 0.03223416114r^4 + 0.002100897817r^6 + 0.00007439596524r^8}} \quad (32)$$

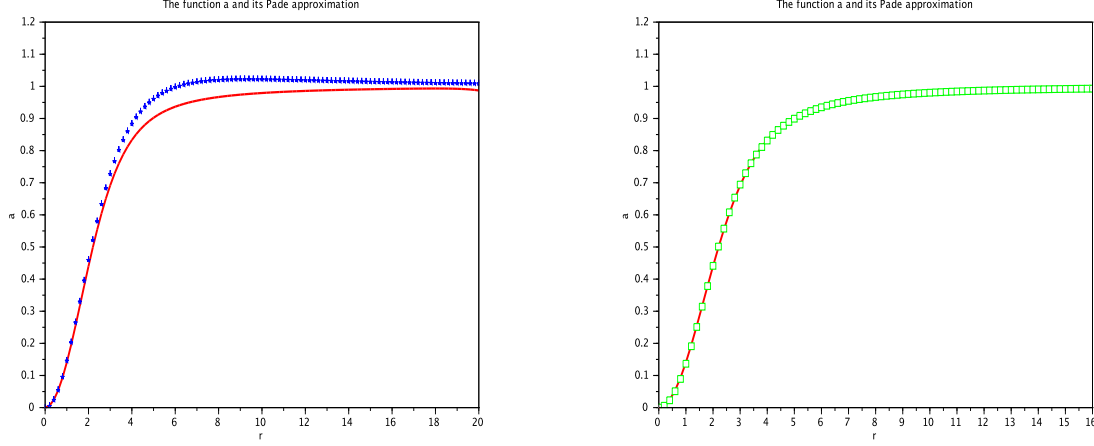


FIGURE 20. Profile of the degree 2 vortex $\mathbf{a}_2^{\text{ref}}$ (continuous red line) and Padé approximants: \mathbf{a}_2^{Be} (30) in blue stars (left); \mathbf{a}_2^{ls} (31) in green squares (right)

	<i>Berloff's</i>	<i>least square</i>
L^2 error	0.1721125	0.0040721
L^∞ error	0.1225094	0.0079088

TABLE 5. Vortex of degree 2 and Padé approximants of higher degree: L^2 and L^∞ errors with the numerical solution obtained with the shooting method.

and with the *least square method*

$$\mathbf{a}_{2bis}^{\text{ls}}(r) \stackrel{\text{def}}{=} r^2 \sqrt{\frac{0.02247580 - 0.0016723r^2 + 0.0002102r^4}{1 + 0.0477937r^2 + 0.0242546r^4 - 0.0008577r^6 + 0.0002102r^8}} \quad (33)$$

with the corresponding plots (see figure 21) and the errors given in table 5. Comparing with \mathbf{a}_2^{Be} , it is noticeable that the L^2 error is almost the same and the L^∞ error is multiplied by 2. If we compare \mathbf{a}_2^{ls} with $\mathbf{a}_{2bis}^{\text{ls}}$, we may notice that the errors are not significantly improved.

4.1.2. Vortex of degree 3

We explore the case of the degree 3 vortex in an analogous way. The approximate asymptotics given by the numerical solution obtained by the shooting method reads now $\mathbf{a}_3^{\text{ref}}(r)/r^3 \rightarrow 0.026183420716$ when $r \rightarrow 0$, *Berloff's method* gives $\mathbf{a}_3^{\text{Be}}(r)/r^3 \rightarrow \sqrt{0.0007951684094} \approx 0.028198731$ and the expression

$$\mathbf{a}_3^{\text{Be}}(r) \stackrel{\text{def}}{=} r^3 \sqrt{\frac{0.0007951684094 + 0.00000864664692r^2}{1 + 0.1358739820r^2 + 0.009952997746r^4 + 0.0005274760603r^6 + 0.00000864664692r^8}}. \quad (34)$$

The *least square method* gives $\mathbf{a}_3^{\text{ls}}(r)/r^3 \rightarrow \sqrt{0.0007568} \approx 0.0275100$ and

$$\mathbf{a}_3^{\text{ls}}(r) \stackrel{\text{def}}{=} r^3 \sqrt{\frac{0.0007568 + 0.0000041r^2}{1 + 0.1846304r^2 + 0.0050719r^4 + 0.0008052r^6 + 0.0000041r^8}} \quad (35)$$

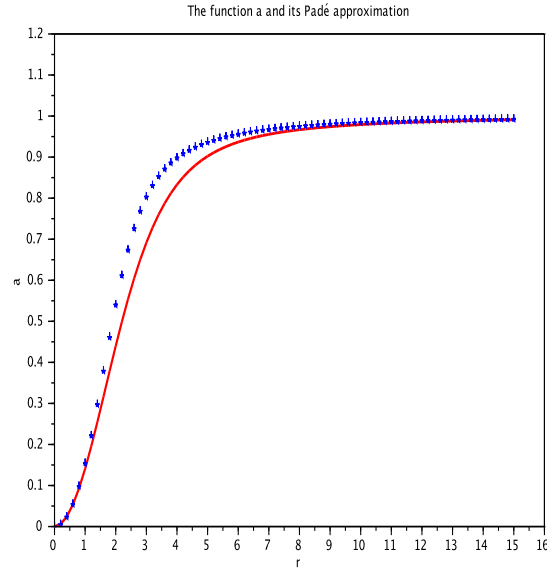


FIGURE 21. Profile of the degree 2 vortex α_2^{ef} (continuous red line) and the Padé approximant of higher degree $\alpha_{2bis}^{\text{Be}}$ (30) (blue stars).

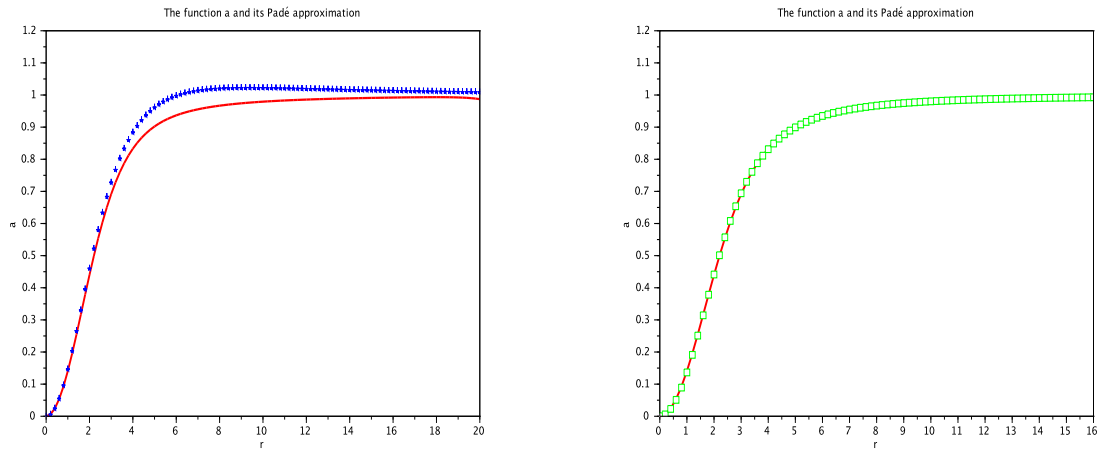


FIGURE 22. Profile of the degree 3 vortex α_3 and Padé approximants: α_3^{Be} (34) in blue stars (left); α_3^{ls} (35) in green squares (right)

We plot these approximations in figure 22 and the errors in table 6.
Same remarks as for the degree 2 vortex hold.

	<i>Berloff's</i>	<i>Least square</i>
L^2 error	0.3215535	0.0062027
L^∞ error	0.1063004	0.0094989

TABLE 6. vortex of degree 3: L^2 and L^∞ errors with the numerical solution obtained with the shooting method.

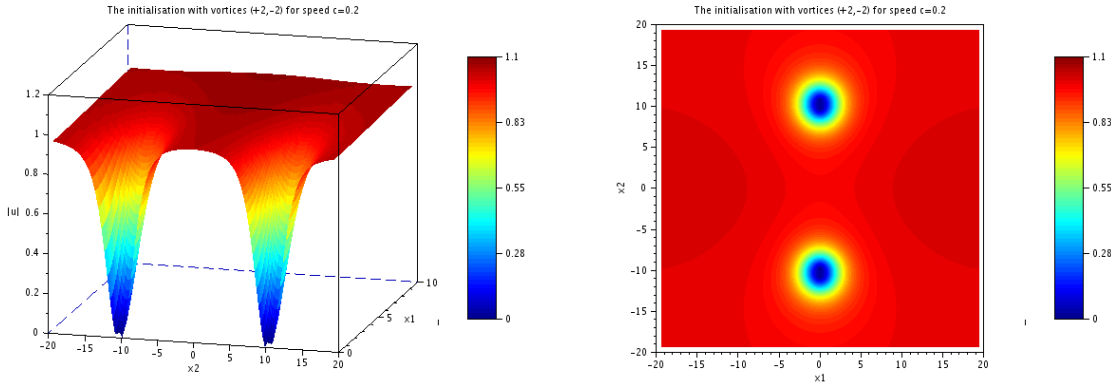


FIGURE 23. Initialization for the $(+2, -2)$ configuration. Modulus on the left and contourplot on the right.

4.1.3. Two vortices configurations

The travelling vortex solution with small speed that we would like to use consists in two vortices of degrees $+n$ and $-n$ at large distance from each other (in a similar way as in the degree one case, see [14] for details). A good approximation of this solution for c small would be given by

$$u_{\pm n \text{ vortices}}^{\text{app}}(x_1, x_2) = \mathbf{a}_n(|(x_1, x_2 - c^{-1})|) \left(\frac{x_1 + i(x_2 - c^{-1})}{|(x_1, x_2 - c^{-1})|} \right)^n \times \mathbf{a}_n(|(x_1, x_2 + c^{-1})|) \left(\frac{x_1 - i(x_2 + c^{-1})}{|(x_1, x_2 + c^{-1})|} \right)^n. \quad (36)$$

We use this expression in order to initialize our continuation algorithm with small speeds.

4.2. $(+2, -2)$ vortex configuration

The $(+2, -2)$ configuration depicted in Figure 23 is obtained by using (36) and the Padé approximant defined in the previous section with the least square method. It is not a travelling wave solution for GP, but has nevertheless allowed us to achieve a numerical solution. Let us mention that the relative residual obtained with the least square Padé approximant is better than Berloff's.

We obtain a new branch of travelling wave solutions using our algorithm. It is remarkable that as the speed decreases the ± 2 vortices split into two ± 1 vortices. The distance between two $+1$ vortices (resp. two -1 vortices) is significantly smaller than the distance between vortices of degree $+1$ and -1 .

Theses solutions are clearly qualitatively different from those on the branches obtained in section 3.

The complete Energy-Momentum diagram augmented with the $(+2, -2)$ branch (in black) is plotted on Figure 25.

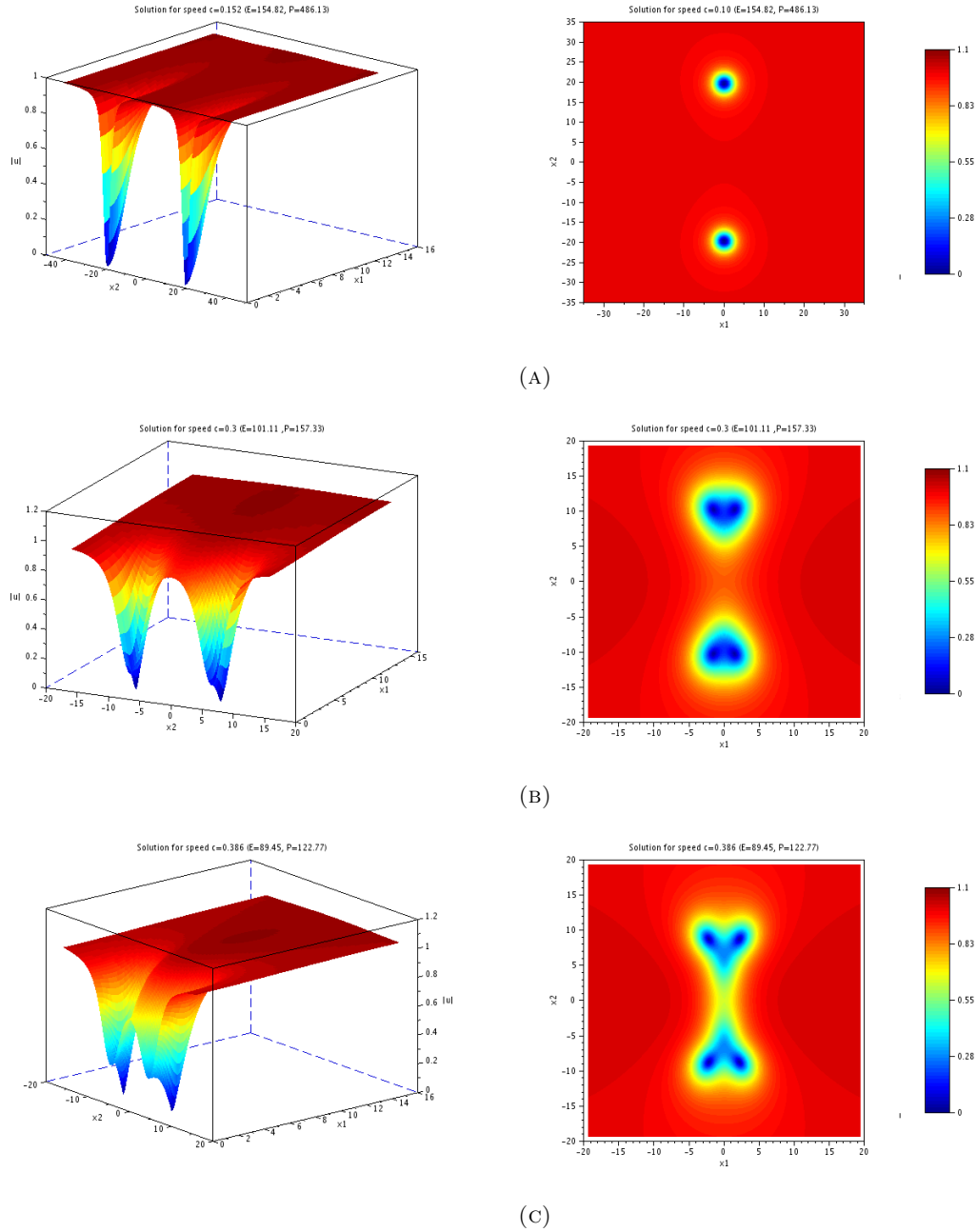


FIGURE 24. Travelling wave associated with the $(+2, -2)$ configuration for speeds: (A) $c = 0.1$; (B) $c = 0.3$; (C) $c = 0.386$. On the left-hand side modulus; on the right-hand side contourplot.

4.3. $(+3, -3)$ vortex configuration

We depict the $(+3, -3)$ configuration for two different speeds in Figures 26 and 27. This time, the initial vortex of degree three splits into three vortices of degree one, in a same way as in the previous subsection. We have then obtained all the branches of the Energy-Momentum diagram of Figure 2.

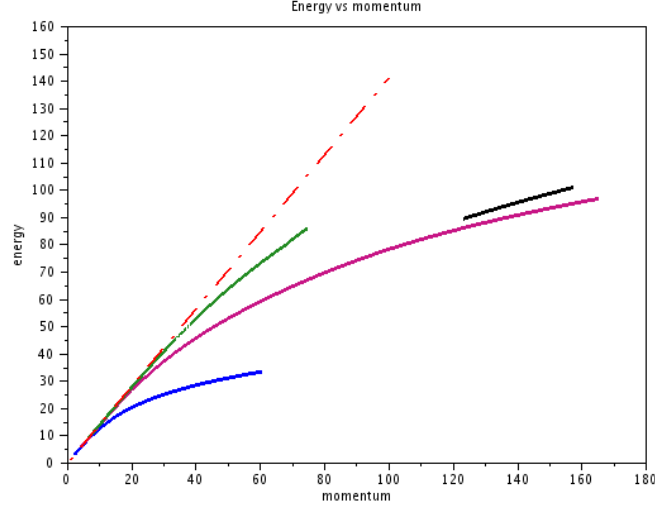


FIGURE 25. Energy-Momentum diagram with the additional branch (in black) associated with the $(+2, -2)$ vortex configuration.

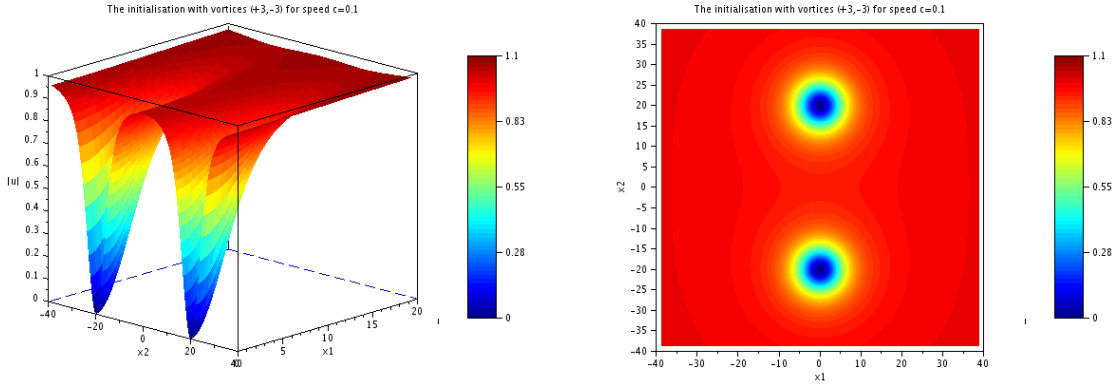


FIGURE 26. Initialization for the $(+3, -3)$ configuration. Modulus on the left and contourplot on the right.

5. CONCLUSION

We have investigated the existence of travelling waves for the two dimensional GP equation. Besides the well-known Jones-Roberts branch, our numerical approach shows the existence of at least four other branches of travelling waves. Two of them are related to the KP-I limit $c \rightarrow c_s$ through the existence (see [27]) of explicit solitary waves for KP-I different from the Lump (the latter being probably the ground state). The last two branches are associated with critical points of the Kirchhoff action involving vortices of degree larger than one.

In a future work, we wish to investigate the dynamical stability issues concerning these travelling waves. The travelling waves on the Jones-Roberts branch are orbitally stable (see [13]), and this is related to the concavity of the curve $P \mapsto E$ combined with the fact that the Hessian of the action $d^2(E - cP)$ has exactly one negative

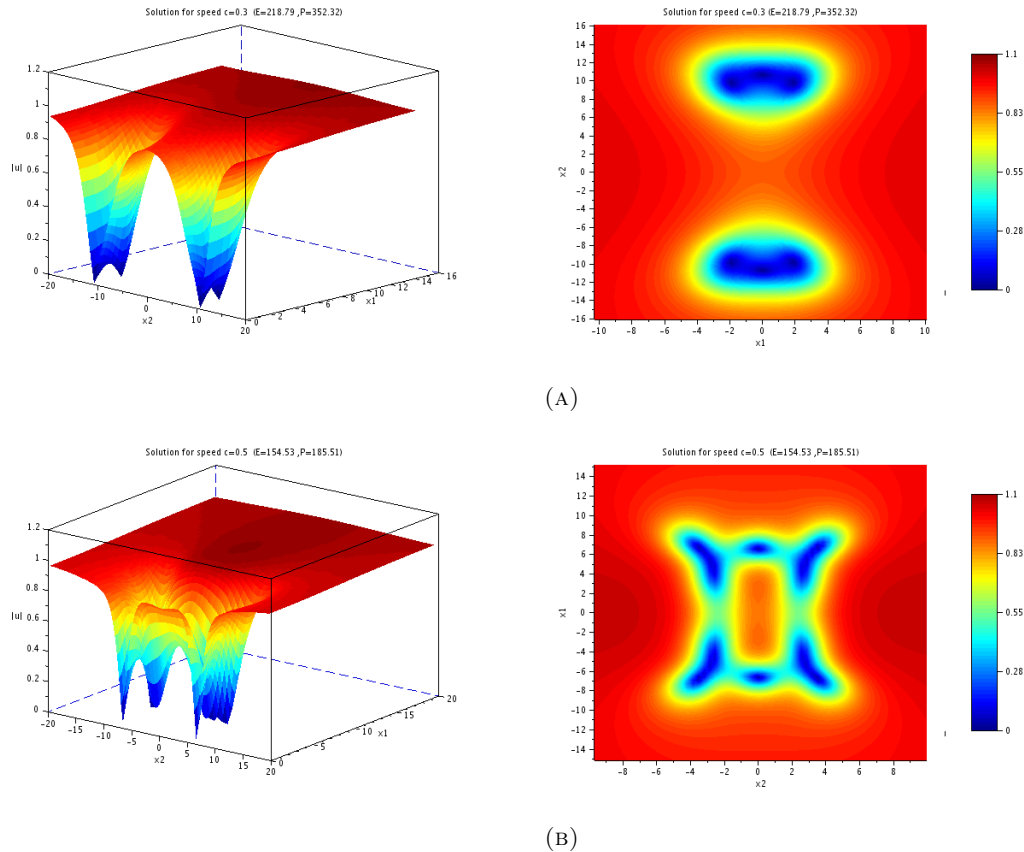


FIGURE 27. Travelling wave associated with the $(+3, -3)$ configuration for speeds: (A) $c = 0.3$; (B) $c = 0.507$. On the left-hand side modulus; on the right-hand side contourplot.

eigenvalue. The situation is actually not very clear for our new branches since there are presumably many negative eigenvalues. We also hope to be able to give some rigorous existence results for these branches.

We are convinced that these new branches also exist in space dimension three, in an axisymmetric setting. For the JR branch, the three dimensional case has already been studied in [21] (see [5, 7, 10, 13, 25] for rigorous mathematical results). In the vortex limit $c \rightarrow 0$, the travelling wave is a vortex ring of large radius. The three dimensional analog of our branch with $(+2, -2)$ or $(+3, -3)$ vortices would then be travelling waves with two or three parallel vortex rings at small distance one from another. This should probably be related to travelling vortex knots in Bose condensates as studied in [29] when the poloidal radius is rather small.

Acknowledgements: This work is supported by the ANR project *BoND* (Bond-ANR-13-BS01-0009-02). We would like to thank Fabrice B ethuel for having raised to D.C. the question of existence of travelling waves to GP with vortices of degree higher than one. At that time, we were looking for solutions with two vortices, one of degree $+2$ and one of degree -2 .

REFERENCES

- [1] M. Abid, C. Huepe, S. Metens, C. Nore, C.T. Pham, L.S. Tuckerman, and M.E. Brachet. Gross-Pitaevskii dynamics of Bose-Einstein condensates and superfluid turbulence. *Fluid Dynamics Research*, 33(5-6):509–544, 2003.

- [2] N. Berloff. Padé approximations of solitary wave solutions of the Gross-Pitaevskii equation. *J. Phys. A: Math. Gen.*, 37(5):1617–1632, 2004.
- [3] F. Bethuel, H. Brezis, and F. Hélein. *Ginzburg-Landau vortices*. Progress in Nonlinear Differential Equations and their Applications, 13. Birkhäuser Boston, Inc., Boston, MA, 1994.
- [4] F. Bethuel, P. Gravejat, and J-C. Saut. On the KP-I transonic limit of two-dimensional Gross-Pitaevskii travelling waves. *Dynamics of PDE*, 5(3):241–280, 2008.
- [5] F. Bethuel, P. Gravejat, and J-C. Saut. Travelling waves for the Gross-Pitaevskii equation. II. *Comm. Math. Phys.*, 285(2):567–651, 2009.
- [6] F. Bethuel, R. L. Jerrard, and D. Smets. On the NLS dynamics for infinite energy vortex configurations on the plane. *Rev. Mat. Iberoam.*, 24(2):671–702, 2008.
- [7] F. Bethuel, G. Orlandi, and D. Smets. Vortex rings for the Gross-Pitaevskii equation. *J. Eur. Math. Soc. (JEMS)*, 6(1):17–94, 2004.
- [8] F. Bethuel and J-C. Saut. Travelling waves for the Gross-Pitaevskii equation. I. *Ann. Inst. H. Poincaré Phys. Théor.*, 70(2):147–238, 1999.
- [9] X. Chen, C. M. Elliott, and T. Qi. Shooting method for vortex solutions of a complex-valued Ginzburg-Landau equation. *Proceedings of the Royal Society of Edinburgh: Section A Mathematics*, 124:1075–1088, 1 1994.
- [10] D. Chiron. Travelling waves for the Gross-Pitaevskii equation in dimension larger than two. *Nonlinear Anal., Theory, Methods, Appl.*, 58(1-2):175–204, 2004.
- [11] D. Chiron. Travelling waves for the Nonlinear Schrödinger Equation with general nonlinearity in dimension one. *Nonlinearity*, 25:813–850, 2012.
- [12] D. Chiron and M. Mariş. Rarefaction pulses for the Nonlinear Schrödinger Equation in the transonic limit. *Comm. Math. Phys.*, 326(2):329–392, 2014.
- [13] D. Chiron and M. Mariş. Travelling waves for the Nonlinear Schrödinger Equation with nonzero condition at infinity. II. to appear in *Arch. Rational Mech. Anal.*, 2017.
- [14] D. Chiron and C. Scheid. Travelling waves for the Nonlinear Schrödinger Equation with general nonlinearity in dimension two. *Journal of Nonlinear Science*, 26(2):171–231, 2016.
- [15] A. de Bouard and J.-C. Saut. Solitary waves of generalized Kadomtsev-Petviashvili equations. *Ann. Inst. H. Poincaré Anal. Non Linéaire*, 14(2):211–236, 1997.
- [16] L. Di Menza. Numerical computation of solitons for optical systems. *M2AN Math. Model. Numer. Anal.*, 43(1):173–208, 2009.
- [17] A. L. Fetter. Vortices in an imperfect Bose Gas. iv. Translational Velocity. *Phys. Rev.*, 151(1):100–104, 1966.
- [18] V. L. Ginzburg and L. P. Pitaevskii. On the theory of superfluidity. *Sov. Phys. JETP*, 7(5):858–861, 1958.
- [19] P. Gravejat. First order asymptotics for the travelling waves in the Gross-Pitaevskii equation. *Adv. Differential Equations*, 11(3):259–280, 2006.
- [20] R.-M. Hervé and M. Hervé. Étude qualitative des solutions réelles d’une équation différentielle liée à l’équation de Ginzburg-Landau. *Ann. Inst. H. Poincaré Anal. Non Linéaire*, 11(4):427–440, 1994.
- [21] C. Jones and P. Roberts. Motion in a Bose condensate IV. Axisymmetric solitary waves. *J. Phys. A: Math. Gen.*, 15:2599–2619, 1982.
- [22] Y. Kivshar and B. Luther-Davies. Dark optical solitons: physics and applications. *Physics Reports*, 298:81–197, 1998.
- [23] H. Lamb. *Hydrodynamics*. Cambridge, UK. Cambridge Univ. Press. 6th ed, 1932.
- [24] S. Manakov, V. Zakharov, L. Bordag, A. Its, and V. Matveev. Two-dimensional solitons of the Kadomtsev-Petviashvili equation and their interaction. *Phys. Lett. A*, 63:205–206, 1977.
- [25] M. Mariş. Traveling waves for nonlinear Schrödinger equations with nonzero conditions at infinity. *Ann. of Math.*, 178:107–182, 2013.
- [26] Y. N. Ovchinnikov and I. M. Sigal. Ginzburg-Landau equation III. Vortex dynamics. *Nonlinearity*, 11(5):1277–1294, 1998.
- [27] D. Pelinovsky and Y. Stepanyants. New multisoliton solutions of the Kadomtsev-Petviashvili equations. *Pis'ma Zh. Eksp. Teor. Fiz.*, 57(1):25–29, 1993.
- [28] L. Pismen. *Vortices in Nonlinear Fields: From Liquid Crystals to Superfluids, From Non-Equilibrium Patterns to Cosmic Strings*. International Series of Monographs on Physics (Book 100). Oxford University Press, 1999.
- [29] D. Proment, M. Onorato, and C. F. Barenghi. Vortex knots in a bose-einstein condensate. *Phys. Rev. E*, 85:036306, 2012.
- [30] P. Roberts and N. Berloff. *Nonlinear Schrödinger equation as a model of superfluid helium*, volume 571 of *Lecture Notes in Physics*. Springer-Verlag, Providence, RI, 2001.
- [31] Z.-Q. Wang and M. Willem. A multiplicity result for the generalized Kadomtsev-Petviashvili equation. *Topol. Methods Nonlinear Anal.*, 7(2):261–270, 1996.
- [32] M. I. Weinstein. On the vortex solutions of some nonlinear scalar field equations. *Rocky Mountain J. Math.*, 21(2):821–827, 1991. Current directions in nonlinear partial differential equations (Provo, UT, 1987).